3-1-2021

Spinal motor neuron loss occurs through a p53-and-p21-independent mechanism in the Smn

Emily J Reedich

Martin Kalski

Nicholas Armijo

Gregory A. Cox
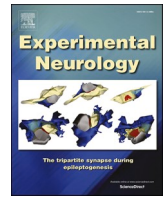*The Jackson Laboratory*, greg.cox@jax.org

Christine J DiDonato

Research paper

Spinal motor neuron loss occurs through a p53-and-p21-independent mechanism in the $Smn^{2B/-}$ mouse model of spinal muscular atrophy

Emily J. Reedich [a,b], Martin Kalski [a], Nicholas Armijo [a], Gregory A. Cox [c,d], Christine J. DiDonato [a,b,*]

[a] Human Molecular Genetics and Physiology Program, Stanley Manne Children's Research Institute at Ann & Robert H. Lurie Children's Hospital, Chicago, IL, USA
[b] Department of Pediatrics, Feinberg School of Medicine, Northwestern University, Chicago, IL, USA
[c] The Jackson Laboratory, Bar Harbor, ME, USA
[d] Graduate School of Biomedical Sciences and Engineering, University of Maine, Orono, ME, USA

ARTICLE INFO

ABSTRACT

Spinal muscular atrophy (SMA) is a pediatric neuromuscular disease caused by genetic deficiency of the survival motor neuron (SMN) protein. Pathological hallmarks of SMA are spinal motor neuron loss and skeletal muscle atrophy. The molecular mechanisms that elicit and drive preferential motor neuron degeneration and death in SMA remain unclear. Transcriptomic studies consistently report p53 pathway activation in motor neurons and spinal cord tissue of SMA mice. Recent work has identified p53 as an inducer of spinal motor neuron loss in severe Δ7 SMA mice. Additionally, the cyclin-dependent kinase inhibitor *P21* (*Cdkn1a*), an inducer of cell cycle arrest and mediator of skeletal muscle atrophy, is consistently increased in motor neurons, spinal cords, and other tissues of various SMA models. p21 is a p53 transcriptional target but can be independently induced by cellular stressors. To ascertain whether p53 and p21 signaling pathways mediate spinal motor neuron death in milder SMA mice, and how they affect the overall SMA phenotype, we introduced *Trp53* and *P21* null alleles onto the $Smn^{2B/-}$ background. We found that p53 and p21 depletion did not modulate the timing or degree of $Smn^{2B/-}$ motor neuron loss as evaluated using electrophysiological and immunohistochemical methods. Moreover, we determined that *Trp53* and *P21* knockout differentially affected $Smn^{2B/-}$ mouse lifespan: p53 ablation impaired survival while p21 ablation extended survival through Smn-independent mechanisms. These results demonstrate that p53 and p21 are not primary drivers of spinal motor neuron death in $Smn^{2B/-}$ mice, a milder SMA mouse model, as motor neuron loss is not alleviated by their ablation.

1. Introduction

The pediatric neuromuscular disease spinal muscular atrophy (SMA) is the leading genetic cause of infant mortality (Crawford and Pardo, 1996). SMA is an autosomal recessive genetic disorder arising from homozygous loss of the *survival motor neuron 1* (*SMN1*) gene with retention of at least one copy of the paralogous gene *SMN2* (Lefebvre et al., 1995). A single nucleotide transition in *SMN2* impedes splicing of the full-length *SMN2* transcript, yielding very low functional SMN protein levels in the absence of *SMN1* (Lorson et al., 1999). *SMN2* copy number varies in the population and is inversely correlated with SMA disease severity (Feldkotter et al., 2002). Individuals with SMA experience progressive weakness, hypotonia, and paralysis of skeletal muscle due to spinal motor neuron degeneration and cell death (Kolb and Kissel, 2015).

The molecular mechanisms underlying motor neuron loss in SMA remain unresolved, yet transcriptomic and mechanistic studies have implicated the tumor suppressor p53 in this process (Jangi et al., 2017; Murray et al., 2015; Nichterwitz et al., 2020; Simon et al., 2017; Simon et al., 2019; Staropoli et al., 2015). p53 is a ubiquitously expressed transcription factor that can initiate pro-survival mechanisms or apoptosis depending on the severity of the cellular stress (Brady and Attardi, 2010; Levine and Oren, 2009). p53 is expressed in motor neurons of Δ7 SMA mice (Simon et al., 2017). Phosphorylation of p53 serine 18, by p38 MAPK activation, was found to be a death-specific marker that selectively occurs in vulnerable SMA motor neurons in this model (Simon et al., 2019). Other transcriptomic studies have identified p53 pathway activation in spinal cord tissue of an antisense oligonucleotide-based, inducible SMA mouse model at 30 days post-induction of the SMA

phenotype (Jangi et al., 2017; Staropoli et al., 2015) and laser-captured motor neurons belonging to vulnerable motor pools of pre-symptomatic $Smn^{2B/-}$ mice (Murray et al., 2015). In these reports, p53 pathway activation is consistently associated with upregulation of the cyclin-dependent kinase inhibitor *P21* (also known as *Cdkn1a*) (Jangi et al., 2017; Murray et al., 2015; Simon et al., 2017; Staropoli et al., 2015), an inducer of cell cycle arrest (Karimian et al., 2016). Increased *P21* expression has further been reported across a wide variety of tissues in differential gene expression studies using various SMA models (Baumer et al., 2009; Cherry et al., 2017; Corti et al., 2008; Nichterwitz et al., 2020; Olaso et al., 2006; Ruggiu et al., 2012; Tadesse et al., 2008; Wu et al., 2011; Zhang et al., 2008; Zhang et al., 2013). Importantly, p21 can mediate pro-apoptotic or pro-survival signaling through p53-dependent or p53-independent mechanisms that are contingent upon the context of insult and cell type (Gartel, 2005; Gartel and Tyner, 2002). p21 depletion studies have not been undertaken in the context of SMA.

Despite consistent reports of p53 pathway activation in SMA models, inhibition of p53 signaling using genetic and pharmacological methods has yielded conflicting results regarding therapeutic benefit. Tsai et al. (2006) ablated *Trp53* in 'Taiwanese' SMA mice and observed no overall impact on survival when looking at the overall population of SMA mice studied; motor neuron loss was not assessed (Tsai et al., 2006). More recently, Simon et al. (2017) demonstrated that partial genetic and pharmacological inhibition of p53 did not impart a survival benefit to Δ7 SMA mice but rescued motor neuron loss (Simon et al., 2017). In contrast, using an inducible genetic approach, Courtney et al. (2019) reduced *Trp53* transcript abundance in $Smn^{2B/-}$ mice by ~50% and observed no mitigation of motor neuron loss; survival was not assessed (Courtney et al., 2019). Taken together, these studies demonstrate that the transcriptional signature associated with SMA includes the p53 signaling pathway, but whether p53 signaling is necessary to elicit spinal motor neuron death across the spectrum of SMA disease severity remains unclear. This lack of clarity might arise from incomplete *Trp53* depletion in the aforementioned study evaluating the impact of p53 reduction in $Smn^{2B/-}$ mice (Courtney et al., 2019).

The $Smn^{2B/-}$ SMA mouse model expresses the hypomorphic Smn^{2B} allele (Hammond et al., 2010) in conjunction with the *Smn* null allele (Schrank et al., 1997); this results in ubiquitously low Smn expression. The Smn^{2B} allele has a GGA to TTT mutation (the "2B" mutation) in an exon splicing enhancer site within exon 7, disrupting exon 7 inclusion in the mature *Smn* transcript (DiDonato et al., 2001). $Smn^{2B/-}$ mice have a slightly milder disease course and are longer-lived than the more commonly utilized Δ7 SMA mouse model (Bowerman et al., 2012; Gogliotti et al., 2013; Le et al., 2005; Quinlan et al., 2019).

Here, we determine whether p53 and p21 are primary mediators of spinal motor neuron loss in less severe SMA mice, using the $Smn^{2B/-}$ model. We demonstrate that partial and complete *Trp53* and *P21* ablation does not modulate the timing of motor unit loss in $Smn^{2B/-}$ mice. Furthermore, we find that p53 and p21 depletion does not rescue spinal motor neuron death or body weight deficits characteristic of $Smn^{2B/-}$ mice, but differentially modifies their survival. p53 ablation impaired survival while p21 ablation enhanced survival through mechanisms that did not alter Smn levels. Since p21 signaling drives skeletal muscle atrophy (Bongers et al., 2015; Fox et al., 2014), we investigated whether extended survival of *P21*-depleted $Smn^{2B/-}$ mice was caused by attenuated muscle atrophy, but this was not the case. Taken together, these results demonstrate that neither p53 nor p21 signaling pathways are primary drivers of spinal motor neuron loss in milder SMA mice, such as the $Smn^{2B/-}$ model, as motor neuron death proceeds with the same degree and swiftness in their absence.

2. Methods

2.1. Ethics statement

All experiments were performed in accordance with the U.S.

National Institutes of Health Guide for Care and Use of Laboratory Animals. Approval from Northwestern University's Institutional Animal Care and Use Committee was obtained for all experiments performed in this study.

2.2. Animal housing and husbandry

Mice were kept in a controlled vivarium in a 12:12 h light-dark photoperiod and monitored for health. $SMN2^{+/+}$; $SMN\Delta7^{+/+}$; $Smn^{+/-}$ mice were purchased from The Jackson Laboratory (Jax stock no. 005025) and maintained in our colony. Intercrossing $SMN2^{+/+}$; $SMN\Delta7^{+/+}$; $Smn^{+/-}$ mice generated Δ7 SMA mice (genotype: $SMN2^{+/+}$; $SMN\Delta7^{+/+}$; $Smn^{-/-}$) and control mice (genotypes: $SMN2^{+/+}$; $SMN\Delta7^{+/+}$; $Smn^{+/+}$ and $SMN2^{+/+}$; $SMN\Delta7^{+/+}$; $Smn^{+/-}$). End-stage Δ7 SMA mice were euthanized when functional death endpoints were reached (20% loss of body weight, inability to right within 30 s after placement in supine position, and/or visible distress).

The official name of the *Smn* null allele (Smn^-) reported by Schrank et al. (1997) and used here on a congenic C57BL/6 background is *FVB. Cg-Smn1^{tm1Msd}* (Schrank et al., 1997) (Jax stock no. 006214). The official name of the Smn^{2B} allele is *B6.129(Cg)-Smn1^{tm1.1Cdid}/J*; it was used in these studies on a congenic C57BL/6 background (Jax stock no. 34285). This allele was generated from the progenitor line Smn^{2B-Neo} (*B6.129-Smn1^{tm1Cdid}*) by removal of the flox-neo cassette (Hammond et al., 2010). Mice expressing the *Trp53* null allele ($Trp53^-$) (Jacks et al., 1994) or the *P21* null allele ($P21^-$) (Deng et al., 1995) on congenic C57BL/6 J backgrounds (official names *Trp53^{tm1Ty}* and *Cdkn1a^{tm1Led}*, respectively) were obtained from The Jackson Laboratory (Jax stock no. 002101 and 016565, respectively) and bred to $Smn^{2B/2B}$ and $Smn^{+/-}$ mice. $Smn^{2B/+}$ (control) and $Smn^{2B/-}$ (SMA) mice expressing $Trp53^{+/+}$, $Trp53^{+/-}$ or $Trp53^{-/-}$ were generated by crossing $Smn^{+/-}$; $Trp53^{+/-}$ or $Smn^{+/-}$; $Trp53^{-/-}$ mice with $Smn^{2B/2B}$; $Trp53^{+/-}$ or $Smn^{2B/2B}$; $Trp53^{-/-}$ mice. Similarly, $Smn^{2B/+}$ and $Smn^{2B/-}$ mice expressing $P21^{+/+}$, $P21^{+/-}$ or $P21^{-/-}$ were generated by breeding $Smn^{+/-}$; $P21^{+/-}$ or $Smn^{+/-}$; $P21^{-/-}$ mice with $Smn^{2B/2B}$; $P21^{+/+}$, $Smn^{2B/2B}$; $P21^{+/-}$, or $Smn^{2B/2B}$; $P21^{-/-}$ mice. At weaning, $Smn^{2B/-}$ mice were weaned with at least one $Smn^{2B/+}$ littermate (if available) and received moist chow three times weekly to assist with food and water intake. Both male and female mice were included in experiments. However, more male mice homozygous for the *Trp53* null allele were included compared to females of the same genotype, due to sex ratio distortion arising from embryonic-lethal developmental defects common to female *Trp53* null mice (Hu et al., 2008).

2.3. Genotyping

DNA extracted from mouse tail biopsies was genotyped using multiplex PCR. Genotyping the *Smn* null allele and Smn^{2B} allele was done as previously described (Gogliotti et al., 2012; Schrank et al., 1997). The *Trp53* null allele was genotyped using a common primer (5′-TGG ATG GTG GTA TAC TCA GAG C), a mutant forward primer (5′-CAG CCT CTG TTC CAC ATA CAC T), and a wild type forward primer (5′-AGG CTT AGA GGT GCA AGC TG). The product sizes of the wild type and knockout alleles were 321 bp and ~ 110 bp, respectively. The *P21* null allele was genotyped using a common forward primer (5′-GTT GTC CTC GCC TC ATC TA), a wild type reverse primer (5′-GCC TAT GTT GGG AAA CCA GA), and a mutant reverse primer (5′-CTG TCC ATC TGC ACG AGA CTA). The sizes of the wild type and knockout amplicons were 240 bp and 447 bp, respectively. The cycling conditions for PCR genotyping of both *Trp53* and *P21* null alleles were: 94 °C/30 s, 63 °C/45 s, 72 °C/45 s, 35 cycles.

2.4. Assessment of $Smn^{2B/-}$ mouse weight and survival

$Smn^{2B/-}$ mice were monitored daily for survival and weight. Functional death was defined as the inability to right within one minute of

placement in a supine position. If functional death endpoint was reached, that day was noted as the date of death in survival analysis. Mice that died perinatally, or from a cage flood, or were unexpectedly missing from the cage, were excluded from survival analyses. In the event of cage flooding, weight measurements obtained the same day and one day after the event were eliminated from weight analysis. Crossing the *Trp53* or *P21* null allele onto the $Smn^{2B/-}$ line frequently produced runts (both in control and SMA mice). Runts were identified as mice weighing less than either 1.9 g at P5 or 3.5 g by P10. These thresholds were selected because they are greater than two standard deviations below the historical mean body weight of $Smn^{2B/-}$ mice at P5 and P10, respectively. All runts, except those so severely runted that death occurred prior to postnatal day (P)6, were included in survival and weight analyses.

2.5. Western blotting

Tissues were dissected and snap frozen on dry ice or liquid nitrogen. Total protein was extracted from homogenized tissues using RIPA buffer supplemented with Halt Protease Inhibitor Cocktail (Thermo Scientific, cat. # 87786), resolved by 10% or 4–12% Bis-Tris polyacrylamide gels using MOPS or MES running buffer, and subsequently transferred to nitrocellulose membranes for western blotting. Ponceau S was applied to visualize total transferred protein levels then the membranes were blocked overnight at 4 °C in Odyssey® Blocking Buffer in PBS (LI-COR, cat. #927–40,000). Membranes were probed with primary antibodies for either two hours (Smn, β-tubulin) or overnight at 4 °C (p53, p21, β-actin, β-tubulin) followed by corresponding secondary antibody incubations for one hour at room temperature. Detection was performed using the LI-COR Odyssey Imaging System. Densitometric quantification was performed using ImageJ software. Details for primary and secondary antibodies utilized in these studies were as follows: p53 immunoblots used 40 µg/sample, rabbit anti-p53 antibody (1:1000, Leica Novacastra, cat. #NCL-L-p53-CM5p), rabbit anti-β-actin antibody (1:1000, LI-COR, cat. #926–42,210) and goat anti-rabbit IgG IRDye® 680RD antibody (1:5000, LI-COR, cat. #926–68,071); Smn immunoblots used 22 µg/sample, mouse anti-Smn antibody (1:2500, BD Biosciences, cat. #610646), goat anti-mouse IgG IRDye® 800CW antibody (1:5000, LI-COR, cat. #926–32,210), rabbit anti-β-tubulin antibody (1:5000, Cell Signaling, cat. #2128), and goat anti-rabbit IgG IRDye® 680RD antibody (1:5000, LI-COR, cat. #926–68,071); p21 immunoblots used 48–50 µg/sample, mouse anti-p21 antibody (1:1000, Santa Cruz, cat. # sc-6246), goat anti-mouse IgG IRDye® 800CW antibody (1:5000, LI-COR, cat. #926–32,210) and either rabbit anti-β-tubulin or β-actin antibody with corresponding secondary antibody as noted above. Specificities of p53 and p21 antibodies were confirmed using protein lysates obtained from *Trp53* and *P21* null tissues. Positive control lysates for p53 and p21 that were included on immunoblots were generated from GL26-luc cells treated for 12–24 h with 1 µM doxorubicin.

2.6. RNA preparation and qRT-PCR analysis

Animals were euthanized and tissues dissected at varying time points. Total RNA was extracted using TRIzol reagent (Invitrogen) and an RNeasy Mini kit (Qiagen, cat. #74106) according to the manufacturer's instructions. RNA concentration was determined using a NanoDrop 2000 spectrophotometer (Thermo Scientific) and sample integrity was confirmed by resolution of 28S and 18S rRNA bands in a 2:1 ratio, respectively, by agarose gel electrophoresis. Samples were treated for DNA contamination using Turbo DNase treatment (Invitrogen, #AM1907) according to the manufacturer's instructions and cDNA was prepared from RNA using a High Capacity cDNA Reverse Transcription kit (Life Technologies #4368814). qRT-PCR reactions were performed with an ABI Quant Studio 3 thermocycler using TaqMan assays and fast master mix (Life Technologies, cat. #4352042) in a 20 µl volume. Each assay was performed at least in duplicate and biological replicates for each group analyzed ranged from $N = 3–4$ samples. Samples with C_q values >35 cycles were considered as having no detectable expression. Data was analyzed using the ΔΔCT method. TaqMan primer/probe assays used in this study were: Gapdh (4352339E), Actin (4352341E), Trp53 (Mm01731290_g1), Cdkn1a (Mm04205640_g1), Fas (Mm0120 4974_m1), Pmaip1 (Mm00451763_m1), Fasl (Mm00438864_m1).

2.7. Electrophysiological studies

Electrophysiological measurements were recorded from mice at ages P12-P18. These included controls and $Smn^{2B/-}$ mice that were wild type, heterozygous or homozygous null for either *Trp53* or *P21*. *Trp53* groups were studied at P12, P14, and P17-18 and *P21* groups were studied at P14. Compound muscle action potential (CMAP) and motor unit number estimation (MUNE) were measured using a portable electrodiagnostic system (Synergy EMG machine; Natus Neurology, Middleton, WI) as previously described in detail (Arnold et al., 2014; Quinlan et al., 2019). In brief, insulated monopolar needles were inserted into the proximal hindlimb to provide sciatic nerve stimulation. Ring electrodes were positioned over the proximal triceps surae muscle to record CMAP amplitude; a reference electrode was placed over the metatarsals. A disposable strip electrode (CareFusion, Middleton, WI) was placed on the tail (or contralateral limb) to serve as the ground electrode. The sciatic nerve was stimulated with single square-wave pulses of 0.1-ms duration. Supramaximal responses were generated maintaining stimulus currents ˂ 10 mA; baseline-to-peak and peak-to-peak CMAP amplitude measurements were obtained.

MUNE was measured using an incremental stimulation technique. Average single motor unit potential (SMUP) amplitude was calculated from 10 incremental responses obtained using submaximal stimulation. The first increment (the minimal all-or-none SMUP response) was evoked by delivering 1-Hz square-wave stimulations at an intensity between 0.21 and 0.70 mA. Stimulation intensity was adjusted in 0.03-mA steps to obtain subsequent incremental responses; incremental responses were distinguished visually in real time to obtain nine additional increments. To be accepted, each increment was required to be: *1)* observed for a total of three duplicate responses; *2)* visually distinct from the prior response; and *3)* at least 25 µV greater than the prior response. The peak-to-peak amplitude of each individual incremental response was calculated by subtracting the amplitude of the prior response. Average peak-to-peak SMUP amplitude was defined as the mean peak-to-peak amplitude of the 10 incremental values. Maximum CMAP amplitude (peak-to-peak) was divided by average peak-to-peak SMUP amplitude to yield the estimated number of motor units (MUNE).

2.8. Spinal cord immunostaining

Spinal cord immunofluorescence experiments utilized P16 $Smn^{2B/+}$ and $Smn^{2B/-}$ mouse cohorts. After euthanasia, spinal cords were exposed by dorsal laminectomy and spinal columns were isolated. Spinal columns were fixed overnight at 4 °C in 2% paraformaldehyde, rinsed in PBS, and cryoprotected in 30% sucrose (in PBS). Spinal cords were freed from underlying spinal columns by blunt dissection, embedded in OCT, and rapidly frozen in dry ice-chilled isopentane. Serial transverse sections from T13-S1 were cut at 12 µm thickness. To avoid repeat counts, every 15th section was used for analysis. Following antigen retrieval, sections were blocked for one hour in 5% donkey serum, 0.5% Triton X-100, and 0.5% glycine (in PBS). Primary antibody incubation was done overnight at 4 °C with goat anti-ChAT antibody (1:100, Millipore, cat. #AB144P) and rabbit anti-p53 antibody (1:1000, Leica Novacastra, cat. # NCL-L-p53-CM5p). Secondary antibody incubations were performed sequentially (each for three hours) at room temperature with Alexa Fluor 594 donkey anti-rabbit antibody (1:250, Life Technologies, cat. # A-11055) then Alexa Fluor 488 donkey anti-goat antibody (1:250, Life Technologies, cat.# A-11029). Nuclei were stained with DAPI. Sections were coverslipped using ProLong™ Diamond Antifade Mountant (Life

Technologies, cat. # P36970) or Aqua-Mount (Lerner Laboratories, cat. #13800). Images were acquired at 5× and 10× using a Leica DMR-HC upright microscope; composite images were stitched using Image Composite Editor (Microsoft). Spinal cord sections from end-stage (P12-P15) Δ7 SMA mice treated in the same manner as above were included as positive controls for p53 immunostaining.

2.9. Muscle weights and myofiber cross-sectional area (CSA) distributions

Quad, calf, and tibialis anterior (TA) muscles were dissected from hindlimbs of P18 control (genotypes: $Smn^{2B/+}$; $P21^{+/+}$ and $Smn^{2B/+}$; $P21^{-/-}$), $Smn^{2B/-}$; $P21^{+/+}$ and $Smn^{2B/-}$; $P21^{-/-}$ mice and weighed using an analytical balance. Muscle weights were normalized to body weight. Unless only one dissected muscle was intact, the left and right quad, calf, and TA normalized muscle weights were averaged for analysis. Muscles were fixed overnight in 2% paraformaldehyde at 4 °C, rinsed in PBS, and cryoprotected in 30% sucrose (in PBS). TA muscles from $Smn^{2B/+}$; $P21^{+/+}$, $Smn^{2B/-}$; $P21^{+/+}$ and $Smn^{2B/-}$; $P21^{-/-}$ mice were dabbed dry, embedded in OCT, and frozen on dry ice. Serial transverse sections from muscle mid-belly were collected at 12 μm thickness. Sections were rehydrated in PBS and blocked for 30 min in 5% goat serum, 0.5% Triton X-100, and 0.5% glycine (in PBS). Primary antibody incubation was performed overnight at 4 °C with rabbit anti-dystrophin antibody (1:250, Abcam, cat. # ab15277). After washing, sections were incubated for two hours at room temperature in secondary antibody solution with Alexa Fluor 594 goat anti-rabbit antibody (1:500, Jackson ImmunoResearch, cat. # 111–545-145). Nuclei were labeled with DAPI then slides were coverslipped using ProLong™ Diamond Antifade Mountant (Life Technologies, cat. # P36970). Images were acquired at 20× and 40× with a Leica DM2500 upright microscope and stitched using Image Composite Editor (Microsoft). TA myofiber CSAs were measured automatically (minimum detection threshold: 10 μm^2) using ImageJ (NIH) with minor manual editing. Myofibers that prominently deviated from *en face* orientation, or were damaged or rolled, were excluded from analysis.

3. Statistical analysis

All statistical analyses were performed using GraphPad Prism (GraphPad Software, San Diego, CA). Survival data was represented with Kaplan-Meier survival curves and statistically significant differences between groups were evaluated using log-rank tests. Weight curves were analyzed by mixed-model two-way ANOVA (with Tukey's tests for main column effects). For all other analyses, unpaired *t*-tests (with Welch's correction, in the event of unequal variances) ordinary one-way ANOVA (with Tukey's post-hoc tests), Brown-Forsythe and Welch ANOVA tests (with Dunnett's T3 multiple comparisons tests) in the event of unequal variances, Kruskal-Wallis one-way ANOVA tests (with Dunn's post-hoc tests) in the event of nonparametric distributions, or two-way ANOVA (with Tukey's post-hoc tests) were performed as needed. *P*-values <0.05 were considered statistically significant.

4. Results

4.1. p53 is upregulated in $Smn^{2B/-}$ motor neurons but not in whole spinal cord lysate

To investigate the p53 pathway in milder forms of SMA, we used $Smn^{2B/-}$ mice in a C57BL/6 genetic background. In our laboratory, the median survival has consistently been 28 days of age. After 28 days of age, SMA mice rapidly progress so that ~25% are alive at 31 days with maximum survival of 39 days (Quinlan et al., 2019). Since prior work has shown that many genes upregulated in SMA motor neurons and spinal cord tissues pertain to cellular stress and p53 pathway activation, we sought to understand their transcriptional activation in $Smn^{2B/-}$ mice throughout the disease course (Jangi et al., 2017; Murray et al., 2015;

Simon et al., 2017; Simon et al., 2019; Staropoli et al., 2015). Hence the expression of several stress-associated transcripts [*P21*, *Phorbol-12-myristate-13-acetate-induced protein 1* (*Pmaip1*), *Fas* and *Fas ligand* (*Fasl*)] was analyzed in whole spinal cord from pre-symptomatic (P5) to what we considered end-stage disease (~P24-28) given the rapid disease course thereafter (Supplemental Fig. 1). We found that *P21* transcripts from the earliest time point analyzed, P5, were already significantly increased compared to control mice with a maximum activation at P12 [4.6 ± 0.8 (SMA) vs. 1.0 ± 0.2 (control)] that decreased over time but remained significantly higher than controls. Generally, we found that all transcripts analyzed (*Pmaip1*, *Fas* and *Fasl*), though not significantly different at P5, had a similar trend of increasing over time in $Smn^{2B/-}$ spinal cords compared to age-matched controls, peaking at P12; this time point corresponds with the onset of overt symptomology in this model. *Pmaip1* was the most significantly increased [4.8 ± 0.3 (SMA) vs. 1.0 ± 0.1 (control)] at P12 and remained high (at 3.2-fold increase) at end-stage disease. These results confirm similar findings in this model and suggest that an increase in these transcripts are associated with an increase in p53 signaling and may be associated with the onset of motor neuron cell death (Courtney et al., 2019; Murray et al., 2015).

Activation of p53 and downstream target genes involved in cell death pathways prominently occurs in spinal motor neurons of severe Δ7 SMA mice; this extends to other spinal neuron populations as disease progresses (Simon et al., 2017). To determine if this is also the case in milder SMA mice, we compared p53 upregulation in $Smn^{2B/-}$ mice to previous reports of p53 activation in Δ7 SMA mice using western blotting (Simon et al., 2017). We recapitulated the finding that p53 is prominently upregulated (2.9-fold) in end-stage Δ7 SMA spinal cord tissue compared to control ($P = 0.0007$) (Fig. 1A). Enhanced p53 expression was not observed in $Smn^{2B/-}$ whole spinal cord lysate at any point during the disease course (Fig. 1B). As motor neurons represent only a fraction of spinal cord cell types, we used immunohistochemistry to specifically evaluate p53 expression in motor neurons. By immunofluorescence, we detected a significant increase in nuclear p53 expression in $Smn^{2B/-}$ lumbar motor neurons compared to control ($P = 0.0285$); Δ7 SMA mice were used as a positive control (Fig. 1C–D). We were not able to determine if phosphorylation of p53 S18 marks vulnerable motor neurons in $Smn^{2B/-}$ mice, as the antibody lots that provided specificity for the Δ7 SMA mouse studies are no longer available, and no other p53 S18 commercially available antibodies are qualified for mouse studies. Overall, we determined that nuclear p53 immunoreactivity in non-motor neurons (ChAT-negative cells) was markedly more abundant in end-stage Δ7 SMA mice compared to P16 $Smn^{2B/-}$ mice; this explains why p53 upregulation was undetectable in $Smn^{2B/-}$ versus Δ7 SMA whole spinal cord lysate by western blotting. Since spinal motor neurons of symptomatic (P16) $Smn^{2B/-}$ mice expressed p53, we postulated that the p53 signaling pathway elicits motor neuron loss in this model, as it does in Δ7 SMA mice (Simon et al., 2017). To test this hypothesis, we bred the *Trp53* null allele onto the $Smn^{2B/-}$ background and determined if p53 depletion plays any role in mitigating motor neuron loss.

4.2. p53 depletion does not alter the timing of motor unit loss in $Smn^{2B/-}$ mice

We used an electrophysiological approach to determine if p53 depletion modulates the onset of motor unit loss in $Smn^{2B/-}$ mice. Specifically, we measured sciatic compound muscle action potential (CMAP) and motor unit number estimation (MUNE). Sciatic CMAP magnitude reflects the amount and size of myofibers innervated by motor axons comprising the sciatic nerve. Sciatic MUNE estimates the number of motor axons, and therefore amount of functional motor neurons, comprising the sciatic nerve (Arnold et al., 2015). We previously reported that MUNE drops at P14 in $Smn^{2B/-}$ mice on an FVB/N genetic background (Quinlan et al., 2019). Sciatic CMAPs of $Smn^{2B/-}$ mice that were either wild type, heterozygous or homozygous null for
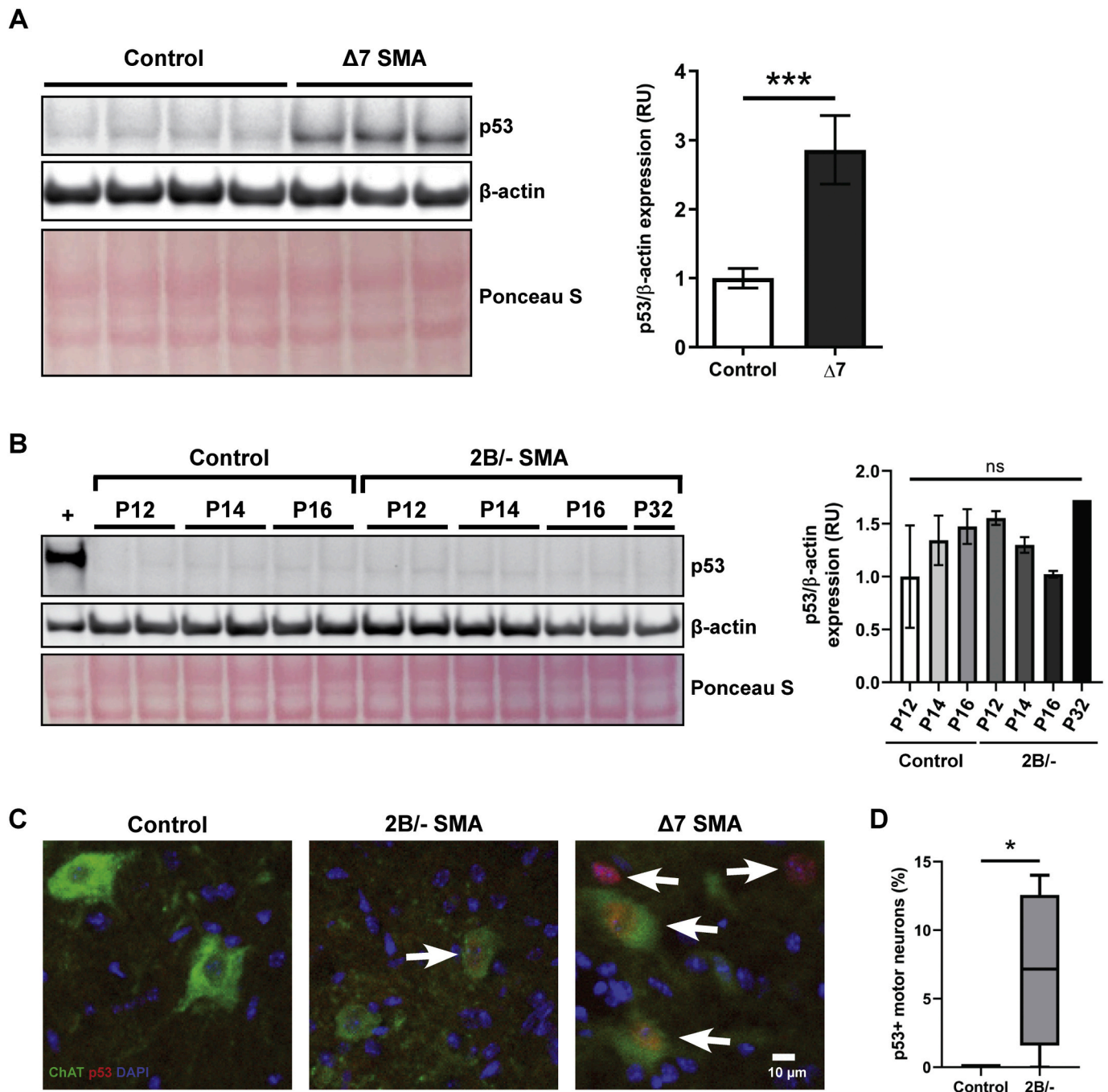
Fig. 1. p53 is upregulated in $Smn^{2B/-}$ and $\Delta 7$ SMA motor neurons. (A) Western blot analysis (left) and densitometric quantification (right) of p53 expression in spinal cord lysate of end-stage $\Delta 7$ SMA mice ($N = 3$) and age-matched controls (N = 4) ($P = 0.0007$, unpaired t-test). Data are represented as mean $\pm$ SD. (B) Western blot analysis (left) and densitometric quantification (right) of p53 in spinal cord lysate of P12-P32 $Smn^{2B/-}$ mice compared to age-matched controls (all $P > 0.05$, one-way ANOVA, Tukey's post-hoc tests). The "+" denotes lysate from doxorubicin-treated GL26-luc cells, that served as a positive control for p53 expression. Data are represented as mean $\pm$ SD. (C) p53 activation and nuclear localization was observed in $Smn^{2B/-}$ lumbar spinal motor neurons using an immunohistochemical approach (exemplified here at P16); $\Delta 7$ SMA motor neurons (shown here at P12) were used as a positive control comparator. White arrows indicate p53-immunoreactive nuclei. (D) p53 nuclear immunoreactivity is significantly increased in lumbar (L4-L6) motor neurons of P16 $Smn^{2B/-}$ mice ($P = 0.0285$, unpaired t-test). Implementation of Welch's correction for unequal variances was used for t-tests when appropriate. For each boxplot, the outlined box represents the interquartile range, the middle bar represents the median, and the error bars reach the minimum and maximum values. $N = 5$–6 per group.

$Trp53$ ($Smn^{2B/-}$; $Trp53^{+/+}$, $Smn^{2B/-}$; $Trp53^{+/-}$ and $Smn^{2B/-}$; $Trp53^{-/-}$) were similar to that of control mice ($Smn^{2B/+}$; $Trp53^{+/+}$) at P12 and P14 (all $P > 0.05$), but were significantly reduced by P17-P18 (all $P < 0.05$) (Fig. 2A). Further, CMAPs were comparable among $Smn^{2B/-}$ groups at all time points (all $P > 0.05$), demonstrating that $Trp53$ knockout did not rescue CMAP diminution in $Smn^{2B/-}$ mice. Moreover, MUNEs of all $Smn^{2B/-}$ groups, regardless of $Trp53$ knockout status, were comparable

to control mice at P12, but were significantly decreased from P14 onward (all $P < 0.05$) (Fig. 2B). MUNEs were equivalent among $Smn^{2B/-}$ cohorts (all $P > 0.05$). Therefore, functional motor unit loss first occurs in C57BL/6 J $Smn^{2B/-}$ mice at P14 (which is equivalent to FVB/N $Smn^{2B/-}$ mice) and $Trp53$ knockout, neither heterozygous nor homozygous, delayed its onset.
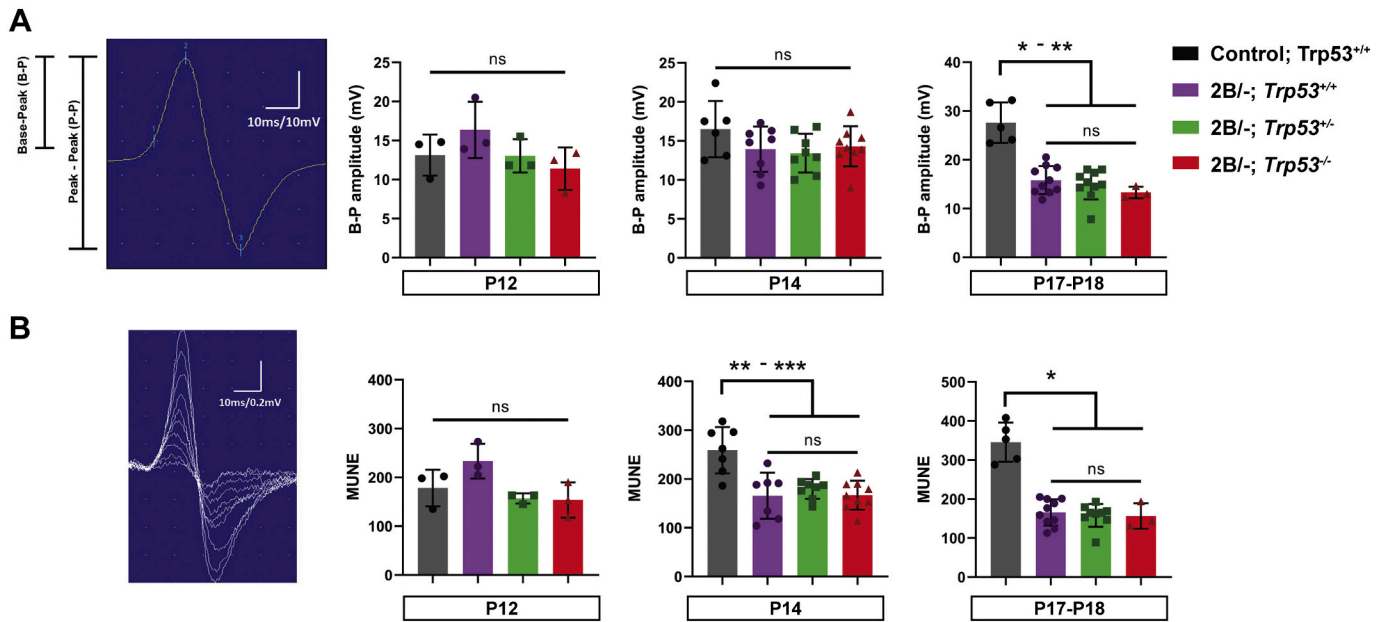
Fig. 2. p53 depletion does not alter the timing of motor unit loss in $Smn^{2B/-}$ mice. (A) Compound muscle action potential (CMAP) schematic and measurements at P12, P14 and P17-P18 for $Smn^{2B/-};Trp53$ background. N = 3–10 mice per group. (B) Motor unit number estimation (MUNE) of mice at P12, P14 and P17-P18. Schematic shows 10 incremental responses (in an SMA mouse). *$P < 0.05$, **$P < 0.01$ and ***$P < 0.001$. Statistical significance was determined using one-way ANOVA with Tukey's post-hoc tests for all datasets except P17-P18 time points, where Kruskal-Wallis one-way ANOVA tests (with Dunn's post-hoc tests) were used due to nonparametric distributions. Data are represented as mean ± SD.

4.3. p53 ablation does not mitigate Smn²ᴮ⁻/⁻ motor neuron loss

Diminished MUNE reflects motor neuron loss, motor axon dysfunction, and neuromuscular junction denervation. To determine if p53-depleted $Smn^{2B/-}$ motor neurons were denervated but not yet lost in the spinal cord, we counted motor neurons in the spinal cord region supplying the sciatic nerve, L4-L6. Consistent with MUNE results, we found that homozygous $Trp53$ deletion did not attenuate spinal motor neuron loss at P16 (Fig. 3). Both $Smn^{2B/-}$; $Trp53^{+/+}$ and $Smn^{2B/-}$; $Trp53^{-/-}$ mice had significantly fewer motor neurons per ventral horn than their respective $Smn^{2B/+}$ control group ($P = 0.0076$ and $P = 0.0054$, respectively) (Fig. 3B). p53 depletion had no partial rescue effect: motor neuron counts were comparable between $Smn^{2B/-}$; $Trp53^{+/+}$ and $Smn^{2B/-}$; $Trp53^{-/-}$ mice ($P = 0.1521$). $Smn^{2B/-}$ motor neurons populating both medial and lateral motor columns were vulnerable to degeneration (Fig. 3C–D). As expected, $Smn^{2B/-}$; $Trp53^{-/-}$ motor neurons did not express p53 (Supplemental Fig. 2). Overall, these results demonstrate that p53 ablation does not prevent $Smn^{2B/-}$ spinal motor neuron death or lessen the degree to which they are lost.

4.4. Trp53 ablation exacerbates Smn²ᴮ⁻/⁻ survival but not body weight

We hypothesized that $Trp53$ deletion would extend $Smn^{2B/-}$ mouse lifespan. Interestingly, we found that $Trp53$ knockout impaired survival of $Smn^{2B/-}$ mice. The median survival of a prior cohort of C57BL/6 J $Smn^{2B/-}$ mice in our colony (historical $Smn^{2B/-}$ mice) and $Smn^{2B/-}$; $Trp53^{+/+}$, $Smn^{2B/-}$; $Trp53^{+/-}$, and $Smn^{2B/-}$; $Trp53^{-/-}$ mice was P28, P29, P24, and P19, respectively (Fig. 4A–B). All $Smn^{2B/-}$ groups exhibited diminished survival compared to pooled $Smn^{2B/+}$ controls (all $P < 0.0001$). Median survival of $Smn^{2B/-}$; $Trp53^{+/+}$ mice was consistent with that of historical $Smn^{2B/-}$ mice (P29 v. P28; $P = 0.4713$), reflecting lack of genetic drift. Heterozygous $Trp53$ knockout significantly impaired survival of Smn²ᴮ⁻; $Trp53^{+/-}$ mice (P24) compared to historical $Smn^{2B/-}$ mice (P28) ($P = 0.0237$), but not compared to $Smn^{2B/-}$; $Trp53^{+/+}$ littermates (P29) ($P = 0.4907$). This discrepancy is likely due

to the small sample size of $Smn^{2B/-}$; $Trp53^{+/+}$ mice versus historical $Smn^{2B/-}$ mice ($N = 12$ v. $N = 35$). However, median survival of $Smn^{2B/-}$; $Trp53^{-/-}$ mice (P19) was drastically reduced compared to both $Smn^{2B/-}$; $Trp53^{+/+}$ littermates (P29) and historical $Smn^{2B/-}$ mice (P28), as well as $Smn^{2B/-}$; $Trp53^{+/-}$ littermates (P24) (all $P < 0.0001$) (Fig. 4A–B). The pronounced survival deficit conferred by p53 depletion was not driven by diminished Smn expression, as $Smn^{2B/-}$ mice that were wild type and homozygous null for $Trp53$ expressed equivalent Smn levels in spinal cord tissue ($P = 1.0$) (Fig. 4C).

We next addressed whether reduced survival of $Trp53$-depleted $Smn^{2B/-}$ mice could have been associated with an inability to obtain nutrition, as we noted that some mice were runted. We assessed body weights as a proxy for this. We first determined that $Trp53$ ablation did not significantly alter growth curves by comparing weights of control mice that were either wild type, heterozygous or homozygous null for $Trp53$ (Fig. 4D). Since there were no differences, we pooled control mice (genotypes: $Smn^{2B/+}$; $Trp53^{+/+}$, $Smn^{2B/+}$; $Trp53^{+/-}$ and $Smn^{2B/+}$; $Trp53^{-/-}$) for further statistical analysis. As expected, growth curves of all $Smn^{2B/-}$ groups, regardless of their $Trp53$ genotype, were significantly different from pooled controls ($P < 0.0001$). Interestingly, there were no differences in growth curves or maximum body weights achieved among the $Smn^{2B/-}$; $Trp53$ genotypes (Fig. 4E–F). However, when historical $Smn^{2B/-}$ body weights were used as a comparator, we did observe a difference between growth curves of historical $Smn^{2B/-}$ and $Smn^{2B/-}$; $Trp53^{+/-}$ mice ($P = 0.0147$), but this had no effect on maximum body weight achieved (Fig. 4F). In support of these results, we note that mice of all SMA genotypes had milk in their stomachs, indicating that they were able to nurse until later stages of disease. Taken together, these findings showed that $Trp53$ ablation modulated $Smn^{2B/-}$ survival, but not weight. Further studies are necessary to identify the underlying cause of the early mortality experienced by $Trp53$-depleted $Smn^{2B/-}$ mice. Specifically, studies that determine whether the early lethality is due to $Trp53$ ablation or potentially a modifier locus coming from the 129S2 congenic interval on $Chrm$ 11 that is linked to the $Trp53$ gene are warranted.
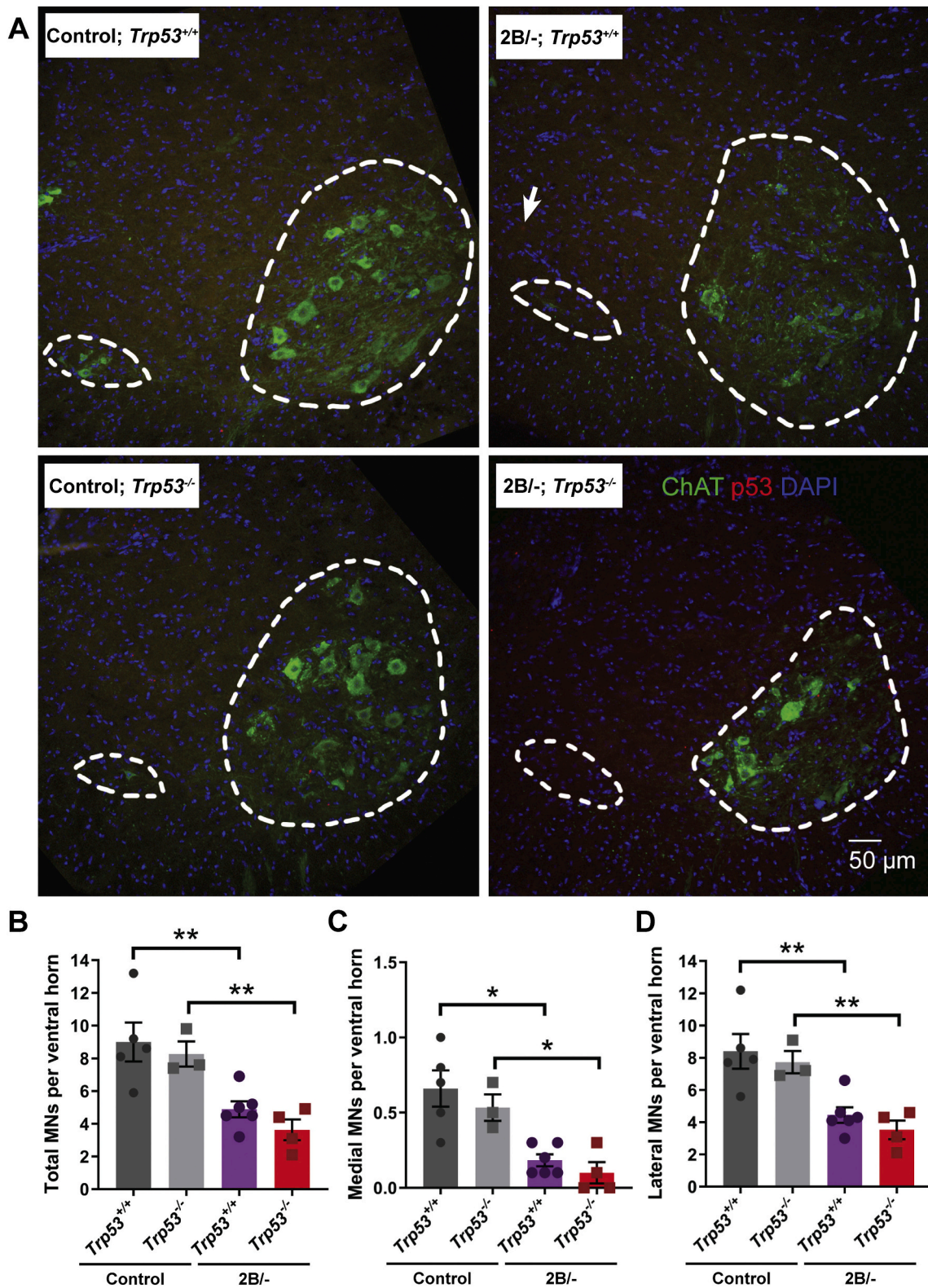
Fig. 3. *Trp53* ablation does not attenuate L4-L6 spinal motor neuron loss in *Smn*$^{2B/-}$ mice. (A) Representative coronal spinal cord sections from P16 *Smn*$^{2B/+}$; *Trp53*$^{+/+}$ and *Smn*$^{2B/+}$; *Trp53*$^{-/-}$ control mice (left) and *Smn*$^{2B/-}$; *Trp53*$^{+/+}$ and *Smn*$^{2B/-}$; *Trp53*$^{-/-}$ SMA mice (right) immunostained for ChAT (green) and p53 (red), with nuclei labeled by DAPI (blue). Medial (MMC) and lateral motor columns (LMC) are outlined in hashed lines. White arrow indicates a p53-immunoreactive nucleus. (B) Quantitative analysis of total motor neurons per ventral horn. *Smn*$^{2B/-}$; *Trp53*$^{+/+}$ and *Smn*$^{2B/-}$; *Trp53*$^{-/-}$ mice both exhibited motor neuron loss at P16, each with fewer motor neurons per ventral horn than their respective controls ($P = 0.0076$ and $P = 0.0054$, respectively, unpaired *t*-test). Both medial (C) and lateral (D) motor columns of *Smn*$^{2B/-}$; *Trp53*$^{+/+}$ and *Smn*$^{2B/-}$; *Trp53*$^{-/-}$ mice had significantly fewer motor neurons compared to their respective controls (*$P < 0.05$, **$P < 0.01$, unpaired t-test). Implementation of Welch's correction for unequal variances was used for t-tests when appropriate. Data are represented as mean ± SEM; N = 3–6 mice per genotype.
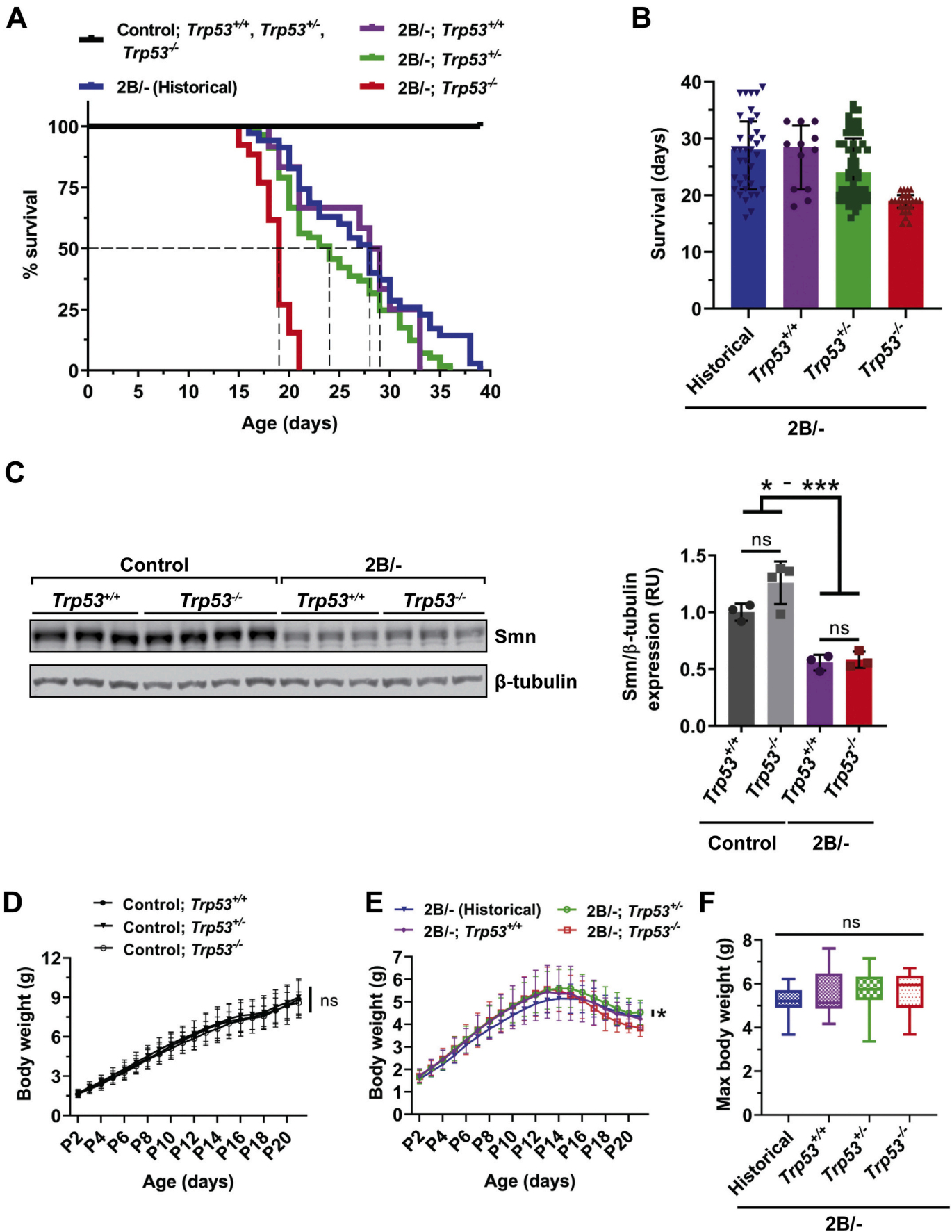
(caption on next page)

Fig. 4. *Trp53* knockout impairs survival of $Smn^{2B/-}$ mice but does not alter their body weight. (A) Kaplan-Meier survival curve of $Smn^{2B/-}$ mice with *Trp53* ablation. Median survival of historical $Smn^{2B/-}$ mice and $Smn^{2B/-}$; $Trp53^{+/+}$, $Smn^{2B/-}$; $Trp53^{+/-}$, and $Smn^{2B/-}$; $Trp53^{-/-}$ mice was P28, P29, P24, and P19, respectively. Survival was impaired in all $Smn^{2B/-}$ groups compared to $Smn^{2B/+}$ controls (all $P < 0.0001$, log-rank test). *Trp53* knockout further diminished survival of $Smn^{2B/-}$ mice: survival of $Smn^{2B/-}$; $Trp53^{-/-}$ mice was significantly reduced compared to both $Smn^{2B/-}$; $Trp53^{+/+}$ littermates and historical $Smn^{2B/-}$ mice as well as $Smn^{2B/-}$; $Trp53^{+/-}$ siblings (all $P < 0.0001$, log-rank tests) and heterozygous *Trp53* knockout significantly impaired survival of $Smn^{2B/-}$; $Trp53^{+/-}$ mice compared to historical $Smn^{2B/-}$ mice ($P = 0.0237$, log-rank test). $N = 76$, $N = 35$, $N = 12$, $N = 57$, and $N = 26$ for $Smn^{2B/+}$; $Trp53^{+/+}$, $Trp53^{+/-}$, $Trp53^{-/-}$ controls, historical $Smn^{2B/-}$ mice, $Smn^{2B/-}$; $Trp53^{+/+}$ mice, $Smn^{2B/-}$; $Trp53^{+/-}$ mice, and $Smn^{2B/-}$; $Trp53^{-/-}$ mice, respectively. (B) Scatter plots depicting the survival distribution of $Smn^{2B/-}$ mice with *Trp53* ablation (same $Smn^{2B/-}$ cohorts as analyzed in A). Data are represented as median ± interquartile range. (C) Western blot analysis (left) and densitometric quantification (right) of Smn expression (normalized to β-tubulin) in spinal cord lysates of P17-P21 $Smn^{2B/+}$ and $Smn^{2B/-}$ mice with and without *Trp53* ablation ($N = 3–4$ per group) were unchanged between $Smn^{2B/+}$; $Trp53^{+/+}$ mice and $Smn^{2B/+}$; $Trp53^{-/-}$ mice and between $Smn^{2B/-}$; $Trp53^{+/+}$ mice and $Smn^{2B/-}$; $Trp53^{-/-}$ mice ($P = 0.0875$ and $P = 1.0$, respectively, one-way ANOVA, Tukey's post-hoc tests). Both $Smn^{2B/-}$ groups exhibited Smn deficiency compared to $Smn^{2B/+}$ control groups (*$P < 0.05$, ***$P < 0.001$, one-way ANOVA, Tukey's post-hoc tests). Data are represented as mean ± SD. (D) *Trp53* knockout did not modulate postnatal day (P)2-P21 $Smn^{2B/+}$ mouse growth (all $P > 0.05$, mixed-model two-way ANOVA, Tukey's tests for main column effect). $N = 13$, $N = 47$, and $N = 16$ for $Smn^{2B/+}$; $Trp53^{+/+}$ mice, $Smn^{2B/+}$; $Trp53^{+/-}$ mice, and $Smn^{2B/+}$; $Trp53^{-/-}$ mice, respectively. Data are represented as mean ± SD. (E) *Trp53* ablation did not improve $Smn^{2B/-}$ mouse growth curves. Weight curves of $Smn^{2B/-}$; $Trp53^{+/+}$, $Smn^{2B/-}$; $Trp53^{+/-}$ and $Smn^{2B/-}$; $Trp53^{-/-}$ mice bred in this study were comparable from P2-P21 (all $P > 0.05$, mixed-model two-way ANOVA, Tukey's tests for main column effect).The only significant difference found in $Smn^{2B/-}$ groups was altered body weight of $Smn^{2B/-}$; $Trp53^{+/-}$ mice compared to historical $Smn^{2B/-}$ mice ($P = 0.0147$, mixed-model two-way ANOVA, Tukey's test for main column effect). $N = 33$, $N = 23$, $N = 57$ and $N = 26$ for historical $Smn^{2B/-}$ mice, $Smn^{2B/-}$; $Trp53^{+/+}$ mice, $Smn^{2B/-}$; $Trp53^{+/-}$ mice, and $Smn^{2B/-}$; $Trp53^{-/-}$ mice, respectively. Data are represented as mean ± SD. (F) Boxplots of maximum body weights reached by P18 historical and $Smn^{2B/-}$ mice that were wild type, heterozygous, or homozygous null for *Trp53*. ns; nonsignificant, all $P > 0.05$, one-way ANOVA, Tukey's post-hoc tests. For each boxplot, the outlined box represents the interquartile range, the middle bar represents the median, and the error bars reach the minimum and maximum values. $N = 33$, $N = 19$, $N = 53$, and $N = 23$ for historical $Smn^{2B/-}$ mice, $Smn^{2B/-}$; $Trp53^{+/+}$ mice, $Smn^{2B/-}$; $Trp53^{+/-}$ mice, and $Smn^{2B/-}$; $Trp53^{-/-}$ mice, respectively.

4.5. P21 knockout does not rescue functional motor unit losses or spinal motor neuron death in Smn²ᴮ/⁻ mice

Prominent *P21* (*Cdkn1a*) transcriptional upregulation, which is present across tissues, is one of the most consistently reported findings in differential gene expression studies using SMA models (Baumer et al., 2009; Corti et al., 2008; Jangi et al., 2017; Murray et al., 2015; Olaso et al., 2006; Ruggiu et al. 2012; Simon et al., 2017; Staropoli et al., 2015; Tadesse et al., 2008; Wu et al., 2011; Zhang et al., 2008; Zhang et al., 2013). It is a downstream transcriptional target of p53 but can also be activated by other cellular stress signals. It is activated when cells are damaged and can regulate cell survival or death. As a first step to understand *P21* transcriptional activation in $Smn^{2B/-}$ spinal cord tissue, we measured *P21* transcript abundance from pre-symptomatic to end-stage of disease using qRT-PCR (Supplemental Fig. 1). We found that *P21* transcripts were very slightly, but significantly, increased in P5 tissue. This steadily increased during early disease but tapered as illness progressed to end-stage (~P24-28). Surprisingly, p21 protein expression was undetectable by western blot analysis using spinal cord extracts from both control and $Smn^{2B/-}$ mice at P16 (Supplemental Fig. 3A). However, using liver tissue from the same animals, we observed both *P21* mRNA and protein upregulation in $Smn^{2B/-}$ mice at P12 and P16, but not in age-matched controls, or p21 knockout mice (Supplemental Fig. 3B). This difference is most likely the result of ~2-fold higher expression of *P21* in liver at P12 and P16 versus spinal cord at P16 in $Smn^{2B/-}$ mice, and the relative heterogenous versus homogenous nature of the tissues. For example, Murray et al. (2015) have demonstrated that *P21* transcripts are more highly expressed in laser-captured motor neurons compared to whole spinal cord tissue from $Smn^{2B/-}$ mice (Murray et al., 2015).

To address whether *P21* activation has a protective or detrimental effect on spinal motor neuron loss and the neuromuscular phenotype of $Smn^{2B/-}$ mice, we genetically ablated *P21*. Homozygous *P21* knockout mice are viable and fertile and were bred onto the $Smn^{2B/-}$ mouse background. Crossing the *P21* null allele onto the $Smn^{2B/-}$ line frequently produced runts (both in controls and SMA mice), similar to the *Trp53* null allele. Like *Trp53* depletion, neither heterozygous nor homozygous *P21* ablation rescued functional motor unit loss (Fig. 5A–B). Sciatic CMAP and MUNE were reduced in P14 $Smn^{2B/-}$; $P21^{+/-}$ and $Smn^{2B/-}$; $P21^{-/-}$ mice compared to $Smn^{2B/+}$; $P21^{+/+}$ controls (all $P < 0.001$). These measures were equally diminished in $Smn^{2B/-}$; $P21^{+/+}$, $Smn^{2B/-}$; $P21^{+/-}$, and $Smn^{2B/-}$; $P21^{-/-}$ mice (all $P > 0.05$), indicating that *P21* knockout yielded no partial rescue effect.

ChAT-immunofluorescence experiments demonstrated that reduced MUNE of p21-depleted $Smn^{2B/-}$ mice reflected spinal motor neuron loss. Compared to $Smn^{2B/+}$; $P21^{-/-}$ littermates, $Smn^{2B/-}$; $P21^{-/-}$ mice had significantly fewer motor neurons at P16 ($P = 0.0250$) (Fig. 5C–E). Lateral motor neurons, which constitute the vast majority of motor neurons in these spinal segments, largely contributed to this result; $Smn^{2B/-}$; $P21^{-/-}$ mice had significantly fewer lateral motor neurons than Smn^{2B+}; $P21^{-/-}$ mice ($P = 0.0064$). There was a trend for reduced numbers of medial motor neurons per ventral horn, but this did not reach statistical significance ($P = 0.2524$) (Fig. 5F–G). We also noted that $Smn^{2B/-}$; $Trp53^{+/+}$; $P21^{+/+}$ and $Smn^{2B/-}$; $P21^{-/-}$ motor neurons had comparable levels of nuclear p53 immunoreactivity ($P = 0.8437$), demonstrating that *P21* ablation did not modulate p53 expression in $Smn^{2B/-}$; $P21^{-/-}$ mice (Supplemental Fig. 2). Taken together, these results demonstrate that p21 depletion, like p53 depletion, did not ameliorate the timing or extent of $Smn^{2B/-}$ spinal motor neuron loss.

4.6. P21 depletion extends survival of Smn²ᴮ/⁻ mice but does not alter body weight

Unlike *Trp53* ablation, *P21* ablation extended survival of $Smn^{2B/-}$ mice. Median survival of historical $Smn^{2B/-}$ mice is 28 days. The median survival of $Smn^{2B/-}$; $P21^{+/+}$, $Smn^{2B/-}$; $P21^{+/-}$, and $Smn^{2B/-}$; $P21^{-/-}$ mice was P34, P33, and P37, respectively (Fig. 6A–B). There was no significant difference between survival of our historical $Smn^{2B/-}$ mice and $Smn^{2B/-}$; $P21^{+/+}$ used here (P34 versus P28; $P = 0.12$). The trend for enhanced survival of $Smn^{2B/-}$; $P21^{+/+}$ mice likely reflects a small sample size ($N = 11$) caused by preferential use of breeding schemes exclusively generating $Smn^{2B/+}$ and $Smn^{2B/-}$ mice with heterozygous and homozygous *P21* knockout. Heterozygous *P21* knockout significantly extended survival of $Smn^{2B/-}$; $P21^{+/-}$ mice (P33) compared to historical $Smn^{2B/-}$ mice (P28) ($P = 0.0481$), but not compared to $Smn^{2B/-}$; $P21^{+/+}$ mice (P34) ($P = 0.9217$). Homozygous *P21* knockout on the SMA background ($Smn^{2B/-}$; $P21^{-/-}$) significantly enhanced survival compared to historical $Smn^{2B/-}$ mice ($P < 0.0001$) and $Smn^{2B/-}$ mice here that were wild type or heterozygous null for *P21* ($P = 0.0462$ and $P = 0.0244$, respectively). Notably, ~40% of $Smn^{2B/-}$; $P21^{-/-}$ mice lived for at least 40 days and ~ 9% more than doubled their lifespan, with the longest surviving mouse reaching 101 days of age. This survival benefit occurred through an Smn-independent mechanism, as Smn levels in $Smn^{2B/-}$; $P21^{-/-}$ spinal cord tissue were equivalent to that of $Smn^{2B/-}$; $P21^{+/+}$ mice ($P = 1.0$) (Fig. 6C).

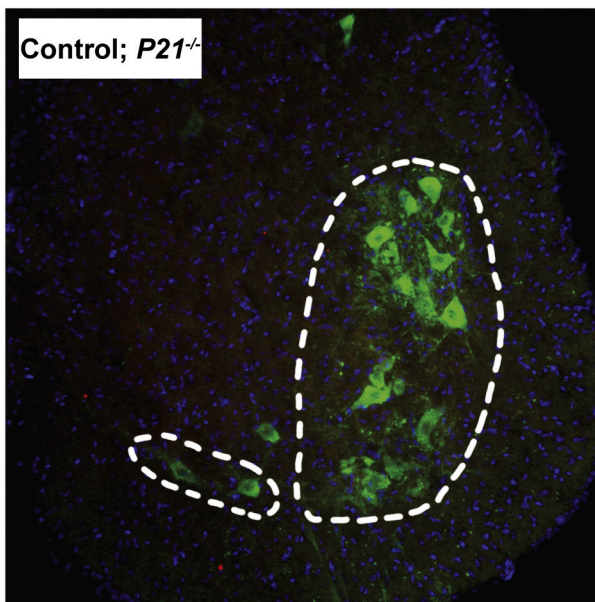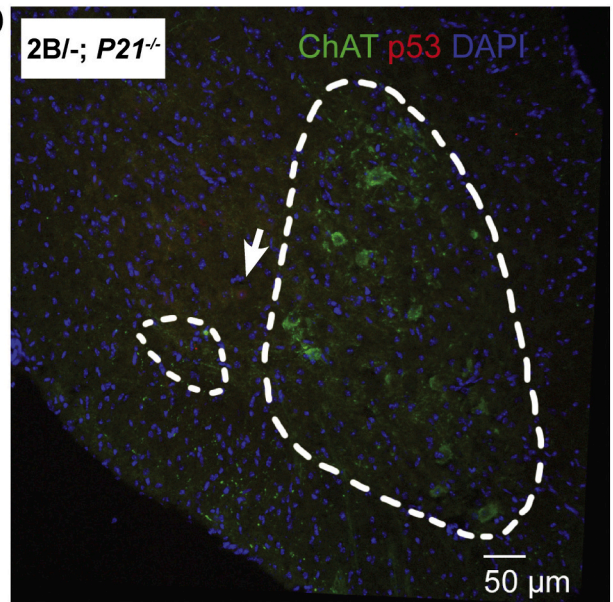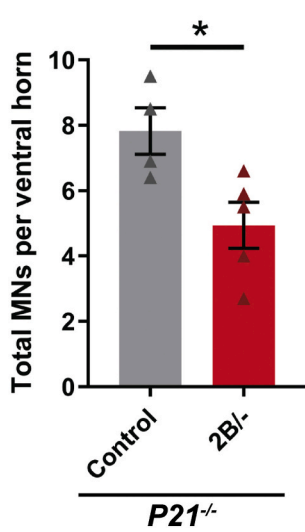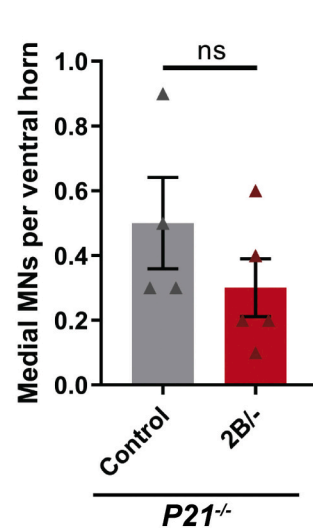Although p21 ablation enhanced survival, it only slightly improved

A

B

C

Control; *P21⁻/⁻*

D

2B/-; *P21⁻/⁻*

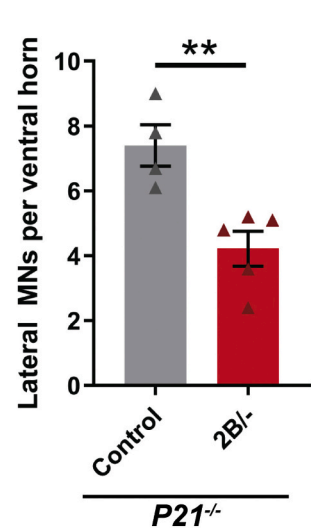ChAT p53 DAPI

50 μm
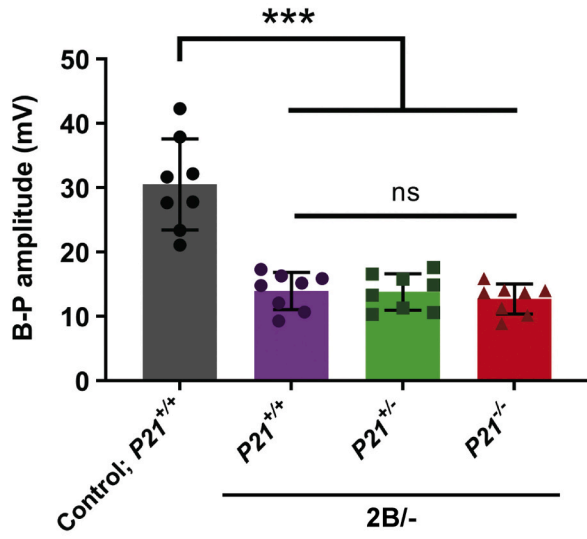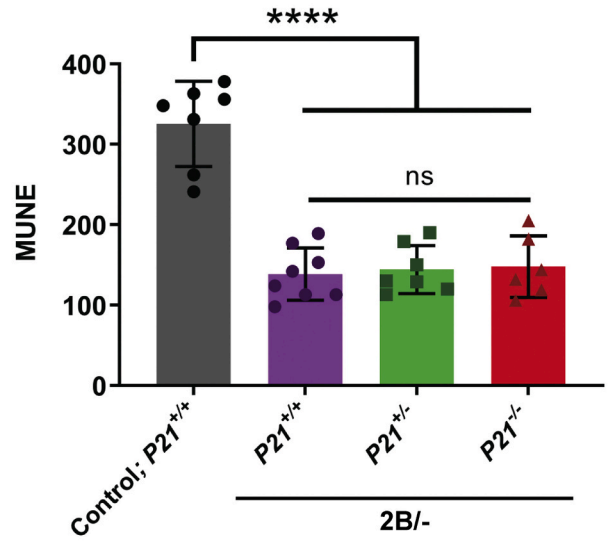
E

F

G

(caption on next page)

Fig. 5. *P21* ablation does not mitigate functional motor unit losses and spinal motor neuron death in *Smn*$^{2B/-}$ mice. (A) Compound muscle action potential (CMAP) and (B) motor unit number estimation (MUNE) were significantly diminished in *Smn*$^{2B/-}$; *P21*$^{+/+}$, *Smn*$^{2B/-}$; *P21*$^{+/-}$, and *Smn*$^{2B/-}$; *P21*$^{-/-}$ mice compared to *Smn*$^{2B/+}$; *P21*$^{+/+}$ mice at P14. CMAP and MUNE were comparable among all *Smn*$^{2B/-}$ groups. ***P < 0.001, Brown-Forsythe and Welch ANOVA tests, Dunnett's T3 multiple comparisons tests; ****P < 0.0001, ordinary one-way ANOVA, Tukey's post-hoc tests. Data are represented as mean ± SD. N = 6–8 mice per group. Representative coronal spinal cord sections from (C) *Smn*$^{2B/+}$; *P21*$^{-/-}$ control and (D) *Smn*$^{2B/-}$; *P21*$^{-/-}$ SMA mice immunostained for ChAT (green) and p53 (red), with nuclei labeled by DAPI (blue). Medial (MMC) and lateral motor columns (LMC) are outlined in hashed lines. White arrow indicates a p53-immunoreactive nucleus. (E) Total motor neurons per ventral horn were significantly less in *Smn*$^{2B/-}$; *P21*$^{-/-}$ mice compared to control *Smn*$^{2B/+}$; *P21*$^{-/-}$ littermates at P16 (*P* = 0.0250, unpaired t-test). (F) There was a trend for fewer medial motor neurons in *Smn*$^{2B/-}$; *P21*$^{-/-}$ mice, but this did not reach statistical significance (*P* = 0.2524, unpaired t-test); (G) lateral motor neurons were significantly reduced in *Smn*$^{2B/-}$; *P21*$^{-/-}$ mice (*P* = 0.0064, unpaired t-test). Data are represented as mean ± SEM; N = 4–5 mice per genotype.

body weight curves of *Smn*$^{2B/-}$ mice during the pre-weaning period. Generally, growth curves of *Smn*$^{2B/-}$ groups were similar, and there were no differences in maximum body weights achieved by P18 (Fig. 6E–F). Starting at P18/19 and increasingly post-weaning, *Smn*$^{2B/-}$; *P21*$^{-/-}$ mice weighed slightly more than both historical *Smn*$^{2B/-}$ mice and *Smn*$^{2B/-}$; *P21*$^{+/+}$ mice bred in this study. This timing coincides with rapid disease progression experienced by *Smn*$^{2B/-}$ mice expressing wild type *P21*. This later-stage weight disparity drove the overall weight curve of *Smn*$^{2B/-}$; *P21*$^{-/-}$ mice to be significantly altered compared to *Smn*$^{2B/-}$; *P21*$^{+/+}$ counterparts (*P* = 0.0128 and *P* = 0.0077, respectively). Overall, *P21* depletion did not correct body weight deficits of *Smn*$^{2B/-}$ mice compared to controls, despite slight improvement of *Smn*$^{2B/-}$; *P21*$^{-/-}$ mouse postnatal growth.

4.7. p21 ablation does not attenuate skeletal muscle atrophy characteristic of Smn$^{2B/-}$ mice

p21 pathway activation in skeletal muscle is caused by a variety of stimuli, including denervation. It induces atrophy by repression of *spermine oxidase* (*Smox*), a positive regulator of muscle mass (Bongers et al., 2015; Fox et al., 2014). Therefore, we hypothesized that inhibition of muscle atrophy, caused by loss of p21, enhanced survival of *Smn*$^{2B/-}$; *P21*$^{-/-}$ mice. To test this, we measured hindlimb skeletal muscle weights and myofiber CSA distributions of P18 control, *Smn*$^{2B/-}$; *P21*$^{+/+}$ and *Smn*$^{2B/-}$; *P21*$^{-/-}$ mice. We found that p21 depletion did not attenuate muscle atrophy in *Smn*$^{2B/-}$ mice (Fig. 7). Average quad, calf, and TA muscle weights (normalized to body weight) were reduced in both *Smn*$^{2B/-}$; *P21*$^{+/+}$ and *Smn*$^{2B/-}$; *P21*$^{-/-}$ mice compared to control (all *P* < 0.05). p21 ablation had no effect on muscle size, as *Smn*$^{2B/-}$; *P21*$^{-/-}$ normalized muscle weights were equivalent to that of *Smn*$^{2B/-}$; *P21*$^{+/+}$ mice (all *P* > 0.05) (Fig. 7B–D). Furthermore, average CSAs of *Smn*$^{2B/-}$; *P21*$^{+/+}$ and *Smn*$^{2B/-}$; *P21*$^{-/-}$ TA myofibers were comparable (*P* = 0.9605) and were smaller than that of *Smn*$^{2B/+}$; *P21*$^{+/+}$ mice (*P* = 0.0132 and *P* = 0.0098, respectively) (Fig. 7E–F). *Smn*$^{2B/-}$; *P21*$^{+/+}$ and *Smn*$^{2B/-}$; *P21*$^{-/-}$ myofiber CSA distributions were alike (Fig. 7G); histogram analysis revealed that the only significant difference in bin frequencies between *Smn*$^{2B/-}$ groups was a greater abundance of 51–100 μm^2-sized myofibers in *Smn*$^{2B/-}$; *P21*$^{-/-}$ mice (*P* = 0.0075) (Fig. 7H). Taken together, these results demonstrate that p21 knockout did not mitigate skeletal muscle atrophy in *Smn*$^{2B/-}$; *P21*$^{-/-}$ mice.

4.8. Pmaip1 transcripts remain significantly elevated in the absence of p53 and p21 in Smn$^{2B/-}$ spinal cord

Our results indicate that p53 and p21 are not the primary drivers of motor neuron loss in *Smn*$^{2B/-}$ spinal cord. In the presence of these proteins we saw that *P21*, *Fas*, *FasL* and *Pmaip1* transcripts were significantly elevated over the entire course of disease (*P21*) or progressed to it. To determine if either p53 or p21 were the primary drivers of these observed increases, we compared the abundance of these transcripts in the presence and absence of these proteins at P12 and P16. We also included *Pidd1* (p53-induced-death-domain protein), also known as *LRDD*, which is positively regulated by p53, involved in cell death and we previously observed was significantly increased in the spinal cords of *Smn*$^{2B/-}$ mice (Cherry et al., 2017). First, we determined

that p21 is not a significant transcriptional activator for *Fas*, *Fasl*, *Pmaip1* or *Pidd1*, as there were no differences in transcript abundance when p21 was present or absent in *Smn*$^{2B/-}$ spinal cord. Further, the results suggest that p53 is the primary driver of increased *P21* transcripts early (at P12), but as disease progresses, other transcriptional activators or modulators of *P21* transcript stability act independently of p53, as evidenced by the significant increase in *P21* transcripts at P16 in *Smn*$^{2B/-}$; *Trp53*$^{-/-}$ spinal cord (Fig. 8). In contrast, we found, that *Pidd1* transcripts in SMA spinal cord were completely p53-regulated, as in its absence, *Pidd1* transcripts remained at control levels. *Fas*, *Fasl* and *Pmaip1* were also positively regulated by p53, as those transcripts returned to baseline control levels at P12. However, similar to *P21* transcripts, as disease progressed, these transcripts increased in abundance, especially *Pmaip1*. In fact, at P16, *Pmaip1* transcripts were 4-fold higher than control samples. Collectively, these data suggest that other transcriptional activators and pathways besides p53 and p21 can induce expression of these genes which are involved in cell death.

5. Discussion

Identifying molecular mechanisms that mediate spinal motor neuron degeneration and loss in SMA will allow these pathways to be targeted therapeutically, yet these mechanisms remain unclear and debated. In this study, we tested whether partial and complete genetic ablation of p53 or p21 rescues functional motor unit losses, spinal motor neuron death, and the SMA phenotype of *Smn*$^{2B/-}$ mice, which have a milder disease course than Δ7 SMA mice. This is an important study, as p53 and p21 are activated under cellular stress conditions; depending on the severity of the stress, in one circumstance they may protect against cell death, and in another circumstance evoke it. We determined that *Trp53* and *P21* knockout had opposing effects on *Smn*$^{2B/-}$ mouse survival and neither meaningfully modulated body weight. Using immunohisto-chemical and electrophysiological approaches, we establish that *Trp53* and *P21* ablation did not modulate the onset or extent of *Smn*$^{2B/-}$ spinal motor neuron death and functional losses. These results unequivocally demonstrate that p53 and p21 are not primary drivers of spinal motor neuron death in the *Smn*$^{2B/-}$ mouse model of SMA. This suggests that in milder SMA mice, p53 and p21-independent mechanisms play an important role in eliciting spinal motor neuron loss.

Our finding that *Trp53* knockout fails to rescue *Smn*$^{2B/-}$ motor neuron loss is consistent with recent work. Courtney et al. (2019) used a tamoxifen-inducible cre-mediated recombination system to knockdown *Trp53* in *Smn*$^{2B/-}$ mice; tamoxifen dosing occurred at P4-P5, achieving approximately 50% reduction in *Trp53* transcript abundance. *Trp53* reduction did not attenuate thoracic *Smn*$^{2B/-}$ motor neuron death at P15 (Courtney et al., 2019). Similarly, we demonstrated that heterozygous *Trp53* deletion did not mitigate onset or degree of lumbar *Smn*$^{2B/-}$ motor neuron loss (at P14-P18). Further, we clearly show that homozygous *Trp53* ablation also does not protect against this loss (Figs. 2–3). Together, these results indicate that spinal motor neuron death occurs through a p53-independent mechanism in *Smn*$^{2B/-}$ mice. In general, motor neurons belonging to both medial and lateral motor columns at L4-L6 appeared similarly susceptible to degeneration in *Smn*$^{2B/-}$ mice, but a stereology study evaluating individual spinal segments of a larger number of animals at multiple time points across the disease course
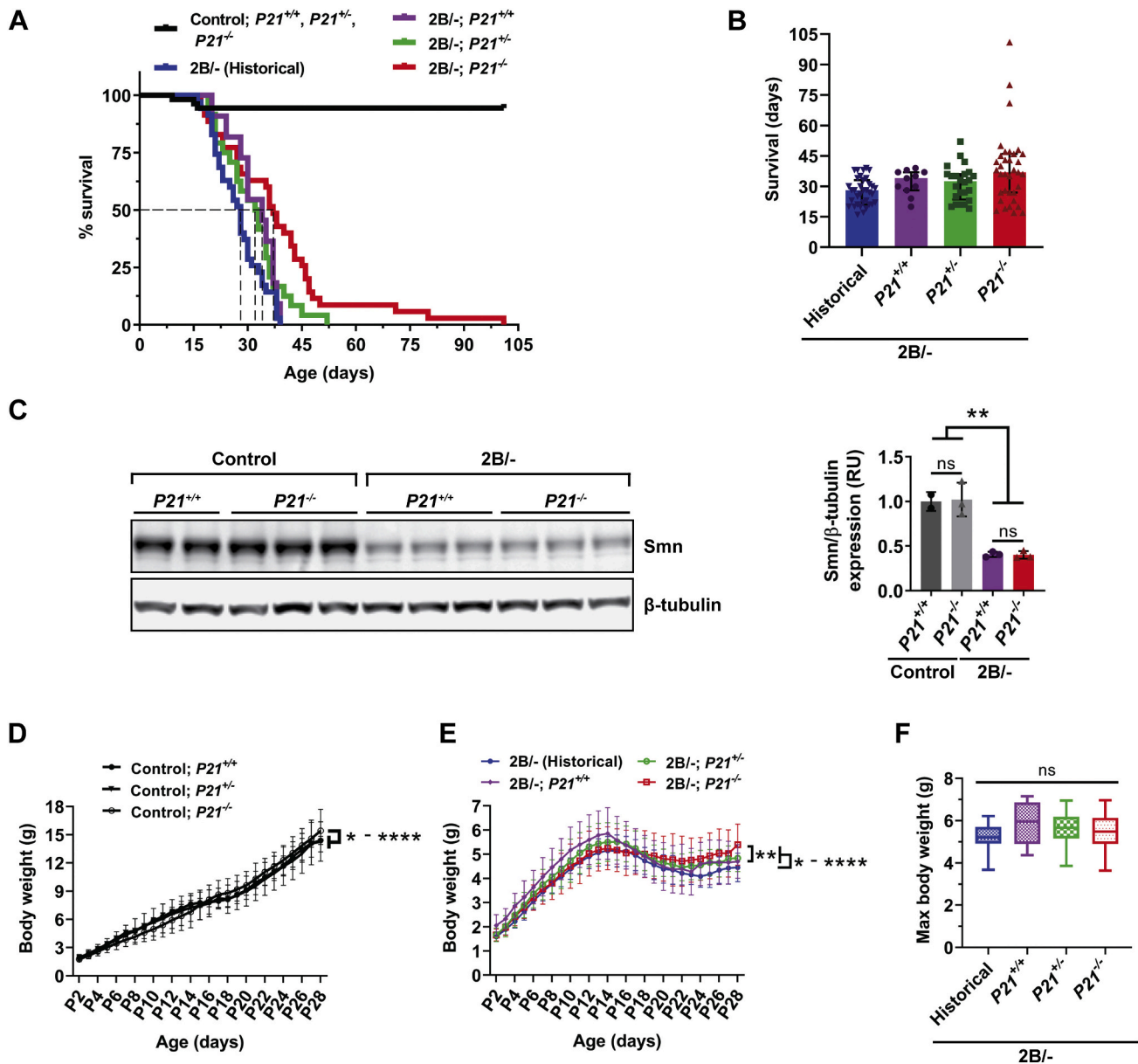
Fig. 6. *P21* knockout confers a significant survival benefit but does not rescue body weight deficits of *Smn*$^{2B/-}$ mice. (A) Kaplan-Meier survival curve of *Smn*$^{2B/-}$ mice with *P21* deletion. Median survival was P28, P34, P33, and P37 for historical *Smn*$^{2B/-}$ mice and *Smn*$^{2B/-}$; *P21*$^{+/+}$, *Smn*$^{2B/-}$; *P21*$^{+/-}$, and *Smn*$^{2B/-}$; *P21*$^{-/-}$ mice, respectively. Survival was significantly reduced in all *Smn*$^{2B/-}$ groups compared to *Smn*$^{2B/+}$ controls (all $P < 0.0001$, log-rank test), yet *P21* ablation extended survival of *Smn*$^{2B/-}$ mice: *Smn*$^{2B/-}$; *P21*$^{-/-}$ mice lived significantly longer than both *Smn*$^{2B/-}$; *P21*$^{+/+}$ littermates and historical *Smn*$^{2B/-}$ mice as well as Smn$^{2B/-}$; *P21*$^{+/-}$ siblings ($P = 0.0462$, $P < 0.0001$, and $P = 0.0244$, respectively) and heterozygous *P21* knockout significantly improved survival of Smn$^{2B/-}$; *P21*$^{+/-}$ mice compared to historical *Smn*$^{2B/-}$ mice ($P = 0.0481$, log-rank test). $N = 54$, $N = 35$, $N = 11$, $N = 24$, and N = 35 for *Smn*$^{2B/+}$; *P21*$^{+/+}$, *P21*$^{+/-}$, *P21*$^{-/-}$ controls, historical *Smn*$^{2B/-}$ mice, *Smn*$^{2B/-}$; *P21*$^{+/+}$ mice, *Smn*$^{2B/-}$; *P21*$^{+/-}$ mice, and *Smn*$^{2B/-}$; *P21*$^{-/-}$ mice, respectively. (B) Scatter plot depicting the survival distribution of *Smn*$^{2B/-}$ mice with *P21* deletion (same *Smn*$^{2B/-}$ cohorts as analyzed in A). Data are represented as median ± interquartile range. (C) Western blot analysis (left) and densitometric quantification (right) of Smn expression (normalized to β-tubulin) in spinal cord lysates of P16 *Smn*$^{2B/+}$ and *Smn*$^{2B/-}$ mice with and without *P21* ablation (N = 2–3 per group). Smn levels between *Smn*$^{2B/+}$; *P21*$^{+/+}$ mice vs. *Smn*$^{2B/+}$; *P21*$^{-/-}$ mice and *Smn*$^{2B/+}$; *P21*$^{+/+}$ mice vs. *Smn*$^{2B/-}$; *P21*$^{-/-}$ mice were similar ($P = 1.0$ and $P = 1.0$, respectively, one-way ANOVA, Tukey's post-hoc tests). Smn expression was significantly diminished in both *Smn*$^{2B/-}$ groups compared to *Smn*$^{2B/+}$ groups (**$P < 0.01$, one-way ANOVA, Tukey's post-hoc tests). Data are represented as mean ± SD. (D) *P21* ablation slightly altered *Smn*$^{2B/+}$ postnatal growth (between P2-P28). The weight curve of *Smn*$^{2B/+}$; *P21*$^{-/-}$ mice was significantly altered compared to *Smn*$^{2B/+}$; *P21*$^{+/+}$ and *Smn*$^{2B/+}$; *P21*$^{+/-}$ mice ($P = 0.0241$ and $P < 0.0001$, respectively, mixed-model two-way ANOVA, Tukey's tests for main column effects). $N = 9$, $N = 17$, and N = 38 for *Smn*$^{2B/+}$; *P21*$^{+/+}$ mice, *Smn*$^{2B/+}$; *P21*$^{+/-}$ mice, and *Smn*$^{2B/+}$; *P21*$^{-/-}$ mice, respectively. Data are represented as mean ± SD. (E) *P21* ablation modulated growth rates within *Smn*$^{2B/-}$ groups. The growth curve of *Smn*$^{2B/-}$; *P21*$^{-/-}$ mice was significantly different than *Smn*$^{2B/-}$;*P21*$^{+/+}$groups (both $P < 0.05$, mixed-model two-way ANOVA, Tukey's tests for main column effects), exemplifying enhanced postnatal growth. *$P < 0.05$, **$P < 0.01$, ****$P < 0.0001$, mixed-model two-way ANOVA, Tukey's test for main column effects. N = 33, $N = 14$, $N = 27$ and N = 43 for historical *Smn*$^{2B/-}$ mice, *Smn*$^{2B/-}$; *P21*$^{+/+}$ mice, *Smn*$^{2B/-}$; *P21*$^{+/-}$ mice, and *Smn*$^{2B/-}$; *P21*$^{-/-}$ mice, respectively. Data are represented as mean ± SD. (F) Boxplots of maximum body weights reached by P18 historical and *Smn*$^{2B/-}$ mice that were wild type, heterozygous, or homozygous null for *P21*. ns; nonsignificant, all $P > 0.05$, one-way ANOVA, Tukey's post-hoc tests. For each boxplot, the outlined box represents the interquartile range, the middle bar represents the median, and the error bars reach the minimum and maximum values. N = 33, $N = 10$, N = 24, and N = 35 for historical *Smn*$^{2B/-}$ mice, *Smn*$^{2B/-}$; *P21*$^{+/+}$ mice, *Smn*$^{2B/-}$; *P21*$^{+/-}$ mice, and *Smn*$^{2B/-}$; *P21*$^{-/-}$ mice, respectively.
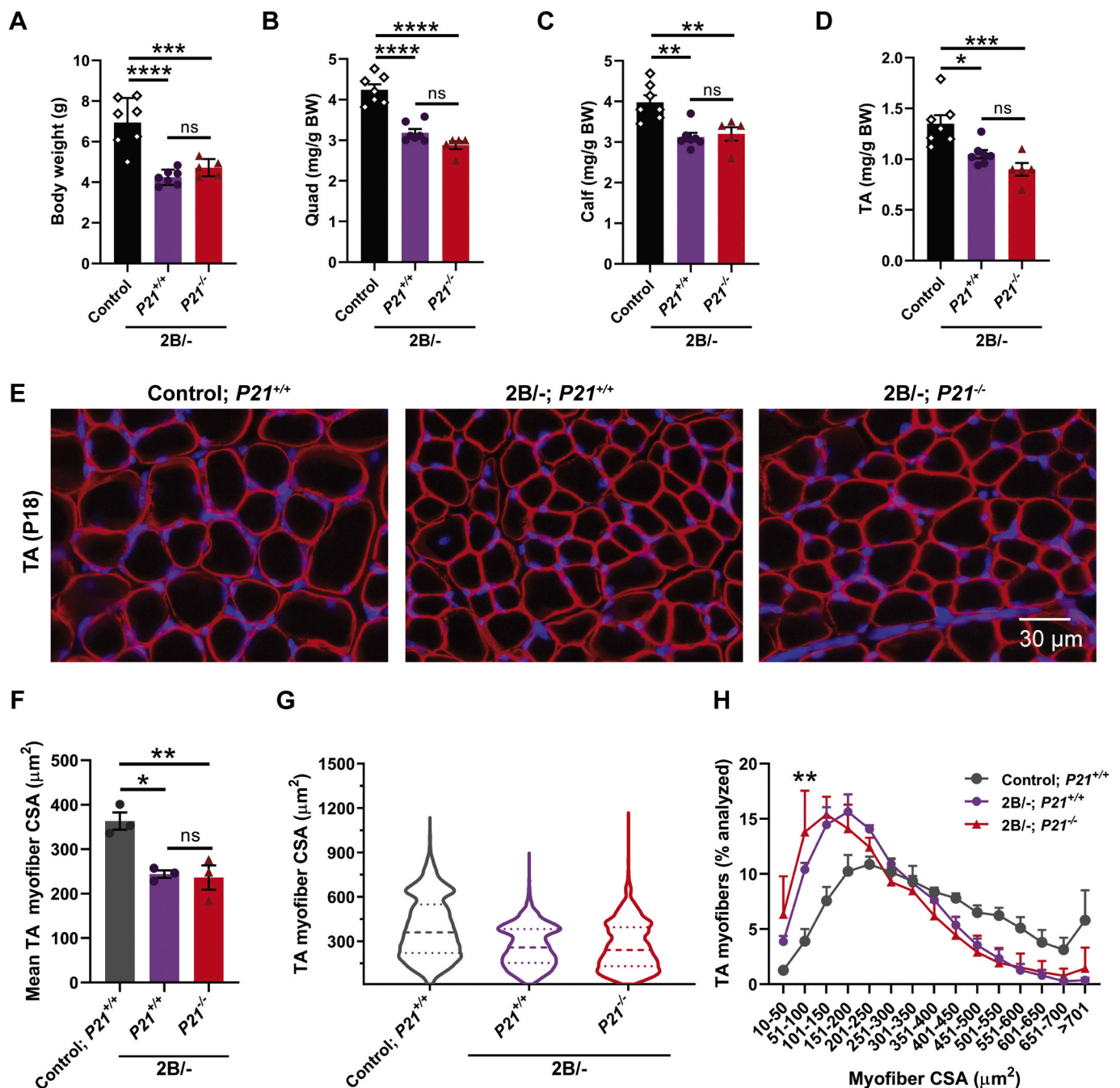
Fig. 7. *P21* ablation does not ameliorate muscle atrophy in P18 *Smn*$^{2B/-}$ mice. (A) Scatter plots of P18 body weights. Both *Smn*$^{2B/-}$; *P21*$^{+/+}$ and *Smn*$^{2B/-}$; *P21*$^{-/-}$ mice weighed less than age-matched controls ($P < 0.0001$ and $P = 0.0006$, respectively, one-way ANOVA, Tukey's post-hoc tests). Body weights of *Smn*$^{2B/-}$; *P21*$^{-/-}$ and *Smn*$^{2B/-}$; *P21*$^{+/+}$ mice were equivalent ($P = 0.5783$, one-way ANOVA, Tukey's post-hoc test). Data are represented as mean ± SD. Mean (B) quad, (C) calf, and (D) TA muscle weights (normalized to body weight) were diminished in *Smn*$^{2B/-}$; *P21*$^{+/+}$ and *Smn*$^{2B/-}$; *P21*$^{-/-}$ mice compared to control (all $P < 0.05$, one-way ANOVA, Tukey's post-hoc tests). *Smn*$^{2B/-}$; *P21*$^{-/-}$ normalized muscle weights were comparable to that of *Smn*$^{2B/-}$; *P21*$^{+/+}$ mice (all $P > 0.05$, one-way ANOVA, Tukey's post-hoc tests). N = 5–7 mice per group. Data are represented as mean ± SEM. (E) Transverse sections of TA muscle from P18 *Smn*$^{2B/+}$; *P21*$^{+/+}$ (left), *Smn*$^{2B/-}$; *P21*$^{+/+}$ (middle), and *Smn*$^{2B/-}$; *P21*$^{-/-}$ (right) mice immunostained for dystrophin (red), with nuclei labeled by DAPI (blue). (F) Mean myofiber CSA was reduced in both *Smn*$^{2B/-}$; *P21*$^{+/+}$ and *Smn*$^{2B/-}$; *P21*$^{-/-}$ TA muscles compared to that of *Smn*$^{2B/+}$; *P21*$^{+/+}$ ($P = 0.0132$ and $P = 0.0098$, respectively, one-way ANOVA, Tukey's post-hoc tests). Mean myofiber CSA of *Smn*$^{2B/-}$; *P21*$^{+/+}$ and *Smn*$^{2B/-}$; *P21*$^{-/-}$ muscles were equivalent ($P = 0.9605$, one-way ANOVA, Tukey's post-hoc test). >1750 myofibers were analyzed per mouse; N = 3 mice per group. Data are represented as mean ± SEM. (G) Violin plots of myofiber CSA distributions in P18 TA muscles. For each violin plot, the hashed line indicates the median, the dotted lines represent interquartile range, and the outer shape depicts the kernel density estimation. (H) Histograms depicting myofiber CSA distributions in P18 TA muscles. Shown are statistics comparing bin frequencies for *Smn*$^{2B/-}$; *P21*$^{+/+}$ and *Smn*$^{2B/-}$; *P21*$^{-/-}$ mice. Frequency distributions were highly similar between *Smn*$^{2B/-}$; *P21*$^{+/+}$ and *Smn*$^{2B/-}$; *P21*$^{-/-}$ mice: the only significant difference was a greater frequency of 51–100 μm²-sized myofibers in *Smn*$^{2B/-}$; *P21*$^{-/-}$ mice ($P = 0.0075$, two-way ANOVA, Tukey's post-hoc test). Data are represented as mean ± SD.
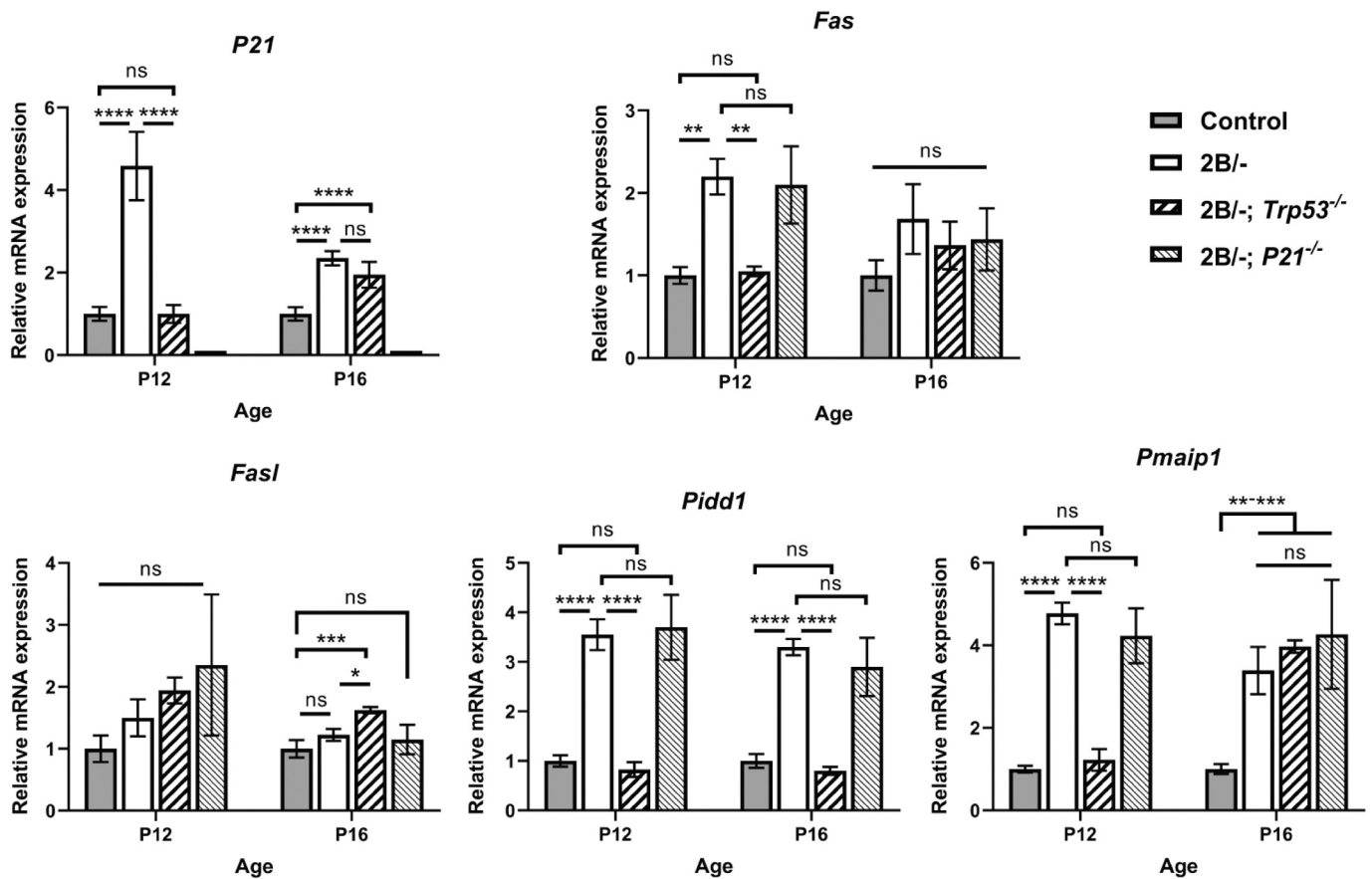
Fig. 8. Effect of p53 or p21 deficiency on gene transcripts involved in cellular stress and cell death. Transcript abundance of *P21* (*Cdkn1a*), *Pmaip1*, *Fas*, *Fasl* and *Pidd1* were analyzed at P12 and P16 in control ($Smn^{2B/+}$) and SMA ($Smn^{2B/-}$) genotypes with and without p53 or p21. Statistical analyses were performed using one-way ANOVA for all transcripts except *Fas*. *Fas* was statistically analyzed using Brown-Forsythe and Welch ANOVA tests (with Dunnett's T3 multiple comparisons tests) since variances were significantly different between groups. The data is presented as mean normalized relative mRNA expression ± SD. N = 3–4 mice per group. (*$P < 0.05$, **$P < 0.01$, ***$P < 0.001$, ****$P < 0.0001$, ns, not significant).

would clarify the phenomenon of preferential vulnerability in this mouse model.

Using the more severe Δ7 SMA mouse model, Simon et al. (2017) reported that SMN deficiency triggers p53 activation early in vulnerable motor neuron pools; resistant motor neuron pools and other (non-motor neuron) cell types that to not degenerate exhibit widespread p53 activation only at later stages of the disease (Simon et al., 2017). They provide compelling evidence that phosphorylation of specific serines in the amino-terminal transactivation domain (TAD) of p53 is necessary to trigger death of vulnerable Δ7 SMA motor neurons, identifying phosphorylation of p53 serine 18 as a death-specific marker that selectively occurs in vulnerable SMA motor neurons. They demonstrated the specificity of these findings using pharmacological inhibition of p53 and shRNA-mediated *Trp53* gene silencing to rescue loss of vulnerable spinal motor neurons in Δ7 SMA mice; resistant motor neurons are not lost during the short lifespan of that mouse (Simon et al., 2017). Interestingly, Nichterwitz et al. (2020) recently demonstrated that both resistant (ocular) and vulnerable (spinal) motor neurons of Δ7 SMA mice upregulate the p53 signaling pathway, signifying cellular stress in both of these somatic motor neuron populations, while resistant neuronal populations (red nucleus neurons and visceral vagus motor neurons) do not exhibit this cellular stress signature (Nichterwitz et al., 2020). The discrepancy between these findings in severe Δ7 SMA mice and our results, plus that of Courtney et al. (2019), suggests that p53 pathway activation (and p53 serine 18 phosphorylation) is necessary to induce motor neuron death in the Δ7 SMA mouse model, but not in the slightly milder $Smn^{2B/-}$ mouse model.

Whether p53 induces pro-survival or pro-apoptotic downstream activity in response to a cellular insult depends on the severity of the cellular stress (Levine and Oren, 2009). Δ7 SMA motor neurons may experience stronger cellular stress than $Smn^{2B/-}$ motor neurons, leading p53 to evoke cell death in the former but not the latter. p53 upregulation in $Smn^{2B/-}$ motor neurons might instead drive protective mechanisms that ultimately fail. The idea of differential cellular stress in these two models is further supported by the timing of motor unit loss (~ one week apart in the models) (Arnold et al., 2014; Quinlan et al., 2019) and the lack of p53 activation that is seen by western blot in $Smn^{2B/-}$ SMA mice versus Δ7 SMA mice. Our findings considered in the broader context of recent reports discussed above, suggest that in patients, spinal motor neuron loss may occur through different molecular mechanisms depending on the severity of SMA clinical symptoms.

Although *Trp53* ablation did not modulate $Smn^{2B/-}$ motor neuron loss, it had a radical effect on $Smn^{2B/-}$ mouse survival. Homozygous *Trp53* knockout shortened the lifespan of $Smn^{2B/-}$; $Trp53^{-/-}$ mice by 10 days when comparing their median survival to $Smn^{2B/-}$; $Trp53^{+/+}$ littermates (P19 v. P29; $P < 0.0001$) (Fig. 4A–B). Since Smn expression itself (Fig. 4C) and motor neuron viability (Figs. 2–3) were unmodified in $Smn^{2B/-}$; $Trp53^{-/-}$ mice, their impaired survival was likely associated with p53 depletion in other cell types. During tissue harvests, we noted that *Trp53*-depleted $Smn^{2B/-}$ mice appeared to have more severe fatty liver and intestinal dysfunction. It is possible that *Trp53* ablation in the liver of $Smn^{2B/-}$; $Trp53^{-/-}$ mice resulted in their early demise. $Smn^{2B/-}$ mice develop impaired fatty acid metabolism and progressively accumulate fat in the liver (termed hepatosteatosis), resembling non-

alcoholic fatty liver disease (NAFLD) (Deguise et al., 2019). Additionally, $Smn^{2B/-}$ mice become hypoglycemic (Deguise et al., 2019), and progressive motor dysfunction likely renders late-stage $Smn^{2B/-}$ mice malnourished. However, we noted that all $Smn^{2B/-}$ mice, regardless of *Trp53* knockout status, had milk in their stomachs until end-stage of disease. It could be that p53 ablation exacerbated metabolic defects in $Smn^{2B/-}$ mice, driving their premature death. Indeed, adult *Trp53* null mice, and mice with liver-specific p53 knockdown, exhibit hepatosteatosis (Jiang et al., 2011; Porteiro et al., 2017; Prokesch et al., 2017; Wang et al., 2013). Chronic, low-dose doxorubicin treatment attenuates hepatosteatosis in NAFLD mice; p53 mediates this attenuation, as doxorubicin treatment failed to ameliorate hepatosteatosis in mice with liver-specific p53-knockdown (Porteiro et al., 2018). Furthermore, in response to food withdrawal, adult mice with liver-specific p53-knockdown become hypoglycemic (reflecting defective glucose homeostasis) and exhibit impaired hepatic amino acid catabolism (Prokesch et al., 2017). Taken together, it is probable that p53 depletion in $Smn^{2B/-}$ mice aggravated liver pathologies, including abnormal fatty acid metabolism and hepatic gluconeogenesis, further impairing their survival. It is also possible that reduced survival is due to a semi-dominant *129S2* modifier on *Chrm* 11 linked to the *Trp53* gene, which we are unable to rule out with these studies. Modifiers are known to exist for SMA and if a modifier did impact survival, it could be specific to liver function or elsewhere.

p53 and other upstream regulators (e.g., Sp1, AP2, and STATs) transactivate *P21* in cellular stress conditions (Gartel and Tyner, 1999; Gorospe et al., 1999; Piccolo and Crispi, 2012). Nuclear subcellular localization enables cell cycle arrest functions of p21, whereas cytoplasmic subcellular localization enables further p21-mediated regulation of cell survival independent of its CDK-inhibitory activity (Cmielova and Rezacova, 2011; Janicke et al., 2007). In a context-dependent manner, p21 mediates both pro-apoptotic and pro-survival signaling relays through p53-dependent and p53-independent mechanisms (Gartel, 2005; Gartel and Tyner, 2002). Although p21 is primarily associated with cell survival responses, evidence for p21's role in driving cell death has emerged (Gartel and Tyner, 2002; Gorospe et al., 1999). Overexpression of p21 has been shown to: (1) induce apoptosis in human cervical cancer, breast carcinoma, and glioma cell lines (Kondo et al., 1996; Sheikh et al., 1995; Tsao et al., 1999); (2) enhance ceramide-induced apoptosis in human hepatocarcinoma cells through upregulation of Bax (Kang et al., 1999); and (3) induce apoptosis in differentiating murine 32Dcl3 myeloblasts upon IL-3 withdrawal (Ghanem and Steinman, 2005). An additional early study demonstrated that *P21* ablation in mouse thymocytes (co-cultured with Fas-ligand-expressing fibroblasts) attenuated Fas-ligand-mediated apoptosis through a p53-independent mechanism (Hingorani et al., 2000). Moreover, p21 associates with and inhibits the anti-apoptotic transcription factors NFκB and STAT3, which may promote apoptosis (Coqueret and Gascan, 2000; Janicke et al., 2007; Khanna et al., 2005). On the other hand, p21 exerts anti-apoptotic functions by associating with and inhibiting pro-apoptotic proteins. These targets include procaspase 3, caspase 8, and ASK-1, an upstream activator of Jun N-terminal kinase (JNK) (Abbas and Dutta, 2009; Asada et al., 1999; Ichijo et al., 1997; Suzuki et al., 1998; Xu and El-Deiry, 2000). Kitaura et al. (2000) demonstrated that p21 suppresses transcriptional activity of c-myc, which might prevent c-myc-mediated apoptosis (Janicke et al., 2007; Kitaura et al., 2000). Lastly, p21 induces expression of secreted anti-apoptotic proteins such as galectin-3 and prosaposin, and addition of conditioned media from p21-induced cells attenuated apoptosis in embryonic mouse fibroblast cells (Chang et al., 2000; Dotto, 2000). In this study, we determine that *P21* deletion, like *Trp53* deletion, did not change the timing or degree of $Smn^{2B/-}$ spinal motor neuron loss (Fig. 5). These results demonstrate that p21 is not necessary to induce $Smn^{2B/-}$ motor neuron death. Rather than inducing cell death, *P21* upregulation in $Smn^{2B/-}$ motor neurons may instead signify a protective response to cellular stress that is ultimately ineffective.

Although *P21* is a well-established transcriptional target of p53, we found that *Trp53* ablation reduced *P21* transcript levels to baseline at P12 in $Smn^{2B/-}$; $Trp53^{-/-}$ mouse spinal cords, but increased with age at P16 (Fig. 8). This result signifies *P21* transcriptional activation by upstream regulators other than p53 or potentially modulation of *P21* transcript stability by regulators such as KRSP, which is dysregulated in SMA (Briata et al., 2005; Tadesse et al., 2008). In addition to p53, numerous other transcription factors induce *P21* expression in response to cellular stress (Gartel and Tyner, 1999; Gorospe et al., 1999). These include: (1) Sp1 and FoxO proteins (in complex with Smad proteins), in response to the cytokine TGF-β (Pardali et al., 2000; Seoane et al., 2004; Zhang et al., 2017); (2) BRCA1, in response to DNA damage (Mullan et al., 2006); (3) members of the Sp1 transcription factor family, (co-activated by p300/CBP) in response to increased intracellular calcium (Missero et al., 1995); (4) AP-2, in response to the phorbol ester tumor promoter, 12-O-tetradecanoylphorbol 13-acetate (TPA) (Zeng et al., 1997); (5) C/EBP-β, in response to antioxidants (Chinery et al., 1997); (6) STATs, in response to the cytokines IFN-α, IL-6, and thrombopoetin (Bellido et al., 1998; Gorospe et al., 1999; Hobeika et al., 1997; Matsumura et al., 1997); and (7) neuronally expressed JAZ, in response to oxidative stress, potassium deprivation-induced neuronal death, and proteinopathies (Mallick and D'Mello, 2014). Numerous additional p53-independent factors induce *P21* expression (in various conditions), including: retinoic acid, vitamin D, vitamin E, androgen, C/EBP-α, GAX, HOXA10, MAPK, nerve growth factor, epidermal growth factor, progesterone, NeuroD, and MyoD1 [reviewed in (Gartel and Tyner, 1999) and (Abbas and Dutta, 2009)]. Cellular stress unfolding in $Smn^{2B/-}$; $Trp53^{-/-}$ spinal cords with age likely evokes *P21* transcription through one or more p53-independent molecular pathways.

Although p21 ablation did not alter $Smn^{2B/-}$ motor neuron viability (Fig. 5) or muscle atrophy (Fig. 7), it considerably extended the lifespan of $Smn^{2B/-}$ mice through mechanisms that did not alter Smn levels (Fig. 6A–C). Notably, ~13% of $Smn^{2B/-}$; $P21^{+/-}$ mice and 40% of $Smn^{2B/-}$; $P21^{-/-}$ mice lived to P40, whereas no $Smn^{2B/-}$; $P21^{+/+}$ littermates or historical $Smn^{2B/-}$ mice did. There are two potential interpretations for this. First, that p21 ablation imparts a survival benefit to $Smn^{2B/-}$ mice through attenuation of pathologies that most likely exist outside the neuromuscular system. However, we performed these analyses at P18 and earlier, and interestingly it is after this age that weight loss in homozygous *P21*-null $Smn^{2B/-}$ mice is not as drastic as either wild type or heterozygous *P21*-null $Smn^{2B/-}$ mice. Hence it would be interesting to determine if *P21* ablation improves muscle mass in SMA models less severe than $Smn^{2B/-}$ mice. The second interpretation for the observed survival benefit could be a modifier locus, which we cannot rule out in the current study. It is possible that a survival modifier is contained within the *129S6* congenic interval on *Chrm* 17 that contains the *P21* knockout allele, or that a negative modifier was lost from the *C57BL/6* background that was present in the region. Again, like *Trp53*, it would be very interesting to know what drives survival either in a negative or positive manner as these are potentially important therapeutic targets. Overall, our work indicates that the primary molecular mechanisms eliciting $Smn^{2B/-}$ motor neuron loss are different than those driving motor neuron loss in Δ7 SMA mice with a more severe neuromuscular phenotype. This is based on our main finding that $Smn^{2B/-}$ motor neuron death proceeds with the same timing and degree in the absence of p53, while p53 pathway inhibition clearly rescues Δ7 SMA motor neuron loss (Simon et al., 2017). Therefore, it is critical to consider where each SMA model system falls along the disease severity spectrum when studying molecular mechanisms of spinal motor neuron dysfunction and death. Moreover, additional studies investigating upstream regulators of spinal motor neuron loss in mouse models milder than Δ7 SMA mice are needed. An additional signaling pathway implicated in initiating Δ7 SMA motor neuron loss is the JNK signaling pathway, as both *Jnk3* knockout and pharmacological treatment with a JNK-inhibitor peptide attenuated the SMA phenotype of Δ7 SMA mice (Genabai et al., 2015; Schellino et al., 2018). Studies testing

involvement of the JNK signaling pathway in $Smn^{2B/-}$ motor neuron death have not been done, but are warranted, since in the absence of p53, *Fas* and *Fasl* increases were noted and they are part of the extrinsic apoptotic pathway regulated by JNK signaling. Similarly, earlier work has identified Fas-ligand-mediated apoptosis in iPSC-derived motor neurons from Type I SMA patients (Sareen et al., 2012), yet Fas-ligand-mediated apoptosis is unexplored in $Smn^{2B/-}$ mice. In addition to these, deficiency in DNA damage repair complexes has been reported in both Δ7 and $Smn^{2B/-}$ SMA mice, providing another pathway that should be further investigated (Kannan et al., 2018; Murray et al., 2015). Further, we show here that *Pmaip1*, which is part of the intrinsic apoptotic pathway, is independently activated in the absence of p53 and would be another excellent target to further evaluate. Overall, the alternative signaling pathways driving $Smn^{2B/-}$ spinal motor neuron death remain to be identified and will have significant implications for supplemental SMA therapies.

Supplementary data to this article can be found online at https://doi.org/10.1016/j.expneurol.2020.113587.

Declaration of Competing Interest

None.

References

Abbas, T., Dutta, A., 2009. p21 in cancer: intricate networks and multiple activities. Nat. Rev. Cancer 9, 400–414. https://doi.org/10.1038/nrc2657.

Arnold, W.D., Porensky, P.N., McGovern, V.L., Iyer, C.C., Duque, S., Li, X., Meyer, K., Schmelzer, L., Kaspar, B.K., Kolb, S.J., Kissel, J.T., Burghes, A.H., 2014. Electrophysiological biomarkers in spinal muscular atrophy: preclinical proof of concept. Ann Clin Transl Neurol 1, 34–44. https://doi.org/10.1002/acn3.23.

Arnold, W.D., Sheth, K.A., Wier, C.G., Kissel, J.T., Burghes, A.H., Kolb, S.J., 2015. Electrophysiological Motor Unit Number Estimation (MUNE) Measuring Compound Muscle Action Potential (CMAP) in Mouse Hindlimb Muscles. J Vis Exp e52899. https://doi.org/10.3791/52899.

Asada, M., Yamada, T., Ichijo, H., Delia, D., Miyazono, K., Fukumuro, K., Mizutani, S., 1999. Apoptosis inhibitory activity of cytoplasmic p21(Cip1/WAF1) in monocytic differentiation. EMBO J. 18, 1223–1234. https://doi.org/10.1093/emboj/18.5.1223.

Baumer, D., Lee, S., Nicholson, G., Davies, J.L., Parkinson, N.J., Murray, L.M., Gillingwater, T.H., Ansorge, O., Davies, K.E., Talbot, K., 2009. Alternative splicing events are a late feature of pathology in a mouse model of spinal muscular atrophy. PLoS Genet. 5, e1000773 https://doi.org/10.1371/journal.pgen.1000773.

Bellido, T., O'Brien, C.A., Roberson, P.K., Manolagas, S.C., 1998. Transcriptional activation of the p21(WAF1,CIP1,SDI1) gene by interleukin-6 type cytokines. A prerequisite for their pro-differentiating and anti-apoptotic effects on human osteoblastic cells. J. Biol. Chem. 273, 21137–21144. https://doi.org/10.1074/jbc.273.33.21137.

Bongers, K.S., Fox, D.K., Kunkel, S.D., Stebounova, L.V., Murry, D.J., Pufall, M.A., Ebert, S.M., Dyle, M.C., Bullard, S.A., Dierdorff, J.M., Adams, C.M., 2015. Spermine oxidase maintains basal skeletal muscle gene expression and fiber size and is strongly repressed by conditions that cause skeletal muscle atrophy. Am. J. Physiol. Endocrinol. Metab. 308, E144–E158. https://doi.org/10.1152/ajpendo.00472.2014.

Bowerman, M., Murray, L.M., Beauvais, A., Pinheiro, B., Kothary, R., 2012. A critical smn threshold in mice dictates onset of an intermediate spinal muscular atrophy phenotype associated with a distinct neuromuscular junction pathology. Neuromuscul. Disord. 22, 263–276. https://doi.org/10.1016/j.nmd.2011.09.007.

Brady, C.A., Attardi, L.D., 2010. p53 at a glance. J. Cell Sci. 123, 2527–2532. https://doi.org/10.1242/jcs.064501.

Briata, P., Forcales, S.V., Ponassi, M., Corte, G., Chen, C.Y., Karin, M., Puri, P.L., Gherzi, R., 2005. p38-dependent phosphorylation of the mRNA decay-promoting factor KSRP controls the stability of select myogenic transcripts. Mol. Cell 20, 891–903. https://doi.org/10.1016/j.molcel.2005.10.021.

Chang, B.D., Watanabe, K., Broude, E.V., Fang, J., Poole, J.C., Kalinichenko, T.V., Roninson, I.B., 2000. Effects of p21Waf1/Cip1/Sdi1 on cellular gene expression: implications for carcinogenesis, senescence, and age-related diseases. Proc. Natl. Acad. Sci. U. S. A. 97, 4291–4296. https://doi.org/10.1073/pnas.97.8.4291.

Cherry, J.J., DiDonato, C.J., Androphy, E.J., Calo, A., Potter, K., Custer, S.K., Du, S., Foley, T.L., Gopalsamy, A., Reedich, E.J., Gordo, S.M., Gordon, W., Hosea, N., Jones, L.H., Krizay, D.K., LaRosa, G., Li, H., Mathur, S., Menard, C.A., Patel, P., Ramos-Zayas, R., Rietz, A., Rong, H., Zhang, B., Tones, M.A., 2017. In vitro and in vivo effects of 2,4 diaminoquinazoline inhibitors of the decapping scavenger enzyme DcpS: context-specific modulation of SMN transcript levels. PLoS One 12, e0185079. https://doi.org/10.1371/journal.pone.0185079.

Chinery, R., Brockman, J.A., Peeler, M.O., Shyr, Y., Beauchamp, R.D., Coffey, R.J., 1997. Antioxidants enhance the cytotoxicity of chemotherapeutic agents in colorectal cancer: a p53-independent induction of p21WAF1/CIP1 via C/EBPbeta. Nat. Med. 3, 1233–1241. https://doi.org/10.1038/nm1197-1233.

Cmielova, J., Rezacova, M., 2011. p21Cip1/Waf1 protein and its function based on a subcellular localization [corrected]. J. Cell. Biochem. 112, 3502–3506. https://doi.org/10.1002/jcb.23296.

Coqueret, O., Gascan, H., 2000. Functional interaction of STAT3 transcription factor with the cell cycle inhibitor p21WAF1/CIP1/SDI1. J Biol Chem 275, 18794–18800. https://doi.org/10.1074/jbc.M001601200.

Corti, S., Nizzardo, M., Nardini, M., Donadoni, C., Salani, S., Ronchi, D., Saladino, F., Bordoni, A., Fortunato, F., Del Bo, R., Papadimitriou, D., Locatelli, F., Menozzi, G., Strazzer, S., Bresolin, N., Comi, G.P., 2008. Neural stem cell transplantation can ameliorate the phenotype of a mouse model of spinal muscular atrophy. J. Clin. Invest. 118, 3316–3330. https://doi.org/10.1172/JCI35432.

Courtney, N.L., Mole, A.J., Thomson, A.K., Murray, L.M., 2019. Reduced P53 levels ameliorate neuromuscular junction loss without affecting motor neuron pathology in a mouse model of spinal muscular atrophy. Cell Death Dis. 10, 515. https://doi.org/10.1038/s41419-019-1727-6.

Crawford, T.O., Pardo, C.A., 1996. The neurobiology of childhood spinal muscular atrophy. Neurobiol. Dis. 3, 97–110. https://doi.org/10.1006/nbdi.1996.0010.

Deguise, M.O., Baranello, G., Mastella, C., Beauvais, A., Michaud, J., Leone, A., De Amicis, R., Battezzati, A., Dunham, C., Selby, K., Warman Chardon, J., McMillan, H. J., Huang, Y.T., Courtney, N.L., Mole, A.J., Kubinski, S., Claus, P., Murray, L.M., Bowerman, M., Gillingwater, T.H., Bertoli, S., Parson, S.H., Kothary, R., 2019. Abnormal fatty acid metabolism is a core component of spinal muscular atrophy. Ann Clin Transl Neurol 6, 1519–1532. https://doi.org/10.1002/acn3.50855.

Deng, C., Zhang, P., Harper, J.W., Elledge, S.J., Leder, P., 1995. Mice lacking p21CIP1/WAF1 undergo normal development, but are defective in G1 checkpoint control. Cell 82, 675–684. https://doi.org/10.1016/0092-8674(95)90039-x.

DiDonato, C.J., Lorson, C.L., De Repentigny, Y., Simard, L., Chartrand, C., Androphy, E. J., Kothary, R., 2001. Regulation of murine survival motor neuron (Smn) protein levels by modifying Smn exon 7 splicing. Hum. Mol. Genet. 10, 2727–2736. https://doi.org/10.1093/hmg/10.23.2727.

Dotto, G.P., 2000. p21(WAF1/Cip1): more than a break to the cell cycle? Biochim. Biophys. Acta 1471, M43–M56. https://doi.org/10.1016/s0304-419x(00)00019-6.

Feldkotter, M., Schwarzer, V., Wirth, R., Wienker, T.F., Wirth, B., 2002. Quantitative analyses of SMN1 and SMN2 based on real-time lightCycler PCR: fast and highly reliable carrier testing and prediction of severity of spinal muscular atrophy. Am. J. Hum. Genet. 70, 358–368. https://doi.org/10.1086/338627.

Fox, D.K., Ebert, S.M., Bongers, K.S., Dyle, M.C., Bullard, S.A., Dierdorff, J.M., Kunkel, S. D., Adams, C.M., 2014. p53 and ATF4 mediate distinct and additive pathways to skeletal muscle atrophy during limb immobilization. Am. J. Physiol. Endocrinol. Metab. 307, E245–E261. https://doi.org/10.1152/ajpendo.00010.2014.

Gartel, A.L., 2005. The conflicting roles of the cdk inhibitor p21(CIP1/WAF1) in apoptosis. Leuk. Res. 29, 1237–1238. https://doi.org/10.1016/j.leukres.2005.04.023.

Gartel, A.L., Tyner, A.L., 1999. Transcriptional regulation of the p21((WAF1/CIP1)) gene. Exp. Cell Res. 246, 280–289. https://doi.org/10.1006/excr.1998.4319.

Gartel, A.L., Tyner, A.L., 2002. The role of the cyclin-dependent kinase inhibitor p21 in apoptosis. Mol. Cancer Ther. 1, 639–649.

Genabai, N.K., Ahmad, S., Zhang, Z., Jiang, X., Gabaldon, C.A., Gangwani, L., 2015. Genetic inhibition of JNK3 ameliorates spinal muscular atrophy. Hum. Mol. Genet. 24, 6986–7004. https://doi.org/10.1093/hmg/ddv401.

Ghanem, L., Steinman, R., 2005. A proapoptotic function of p21 in differentiating granulocytes. Leuk. Res. 29, 1315–1323. https://doi.org/10.1016/j.leukres.2005.03.018.

Gogliotti, R.G., Quinlan, K.A., Barlow, C.B., Heier, C.R., Heckman, C.J., Didonato, C.J., 2012. Motor neuron rescue in spinal muscular atrophy mice demonstrates that sensory-motor defects are a consequence, not a cause, of motor neuron dysfunction. J. Neurosci. 32, 3818–3829. https://doi.org/10.1523/JNEUROSCI.5775-11.2012.

Gogliotti, R.G., Cardona, H., Singh, J., Bail, S., Emery, C., Kuntz, N., Jorgensen, M., Durens, M., Xia, B., Barlow, C., Heier, C.R., Plasterer, H.L., Jacques, V., Kiledjian, M., Jarecki, J., Rusche, J., DiDonato, C.J., 2013. The DcpS inhibitor RG3039 improves survival, function and motor unit pathologies in two SMA mouse models. Hum. Mol. Genet. 22, 4084–4101. https://doi.org/10.1093/hmg/ddt258.

Gorospe, M., Wang, X., Holbrook, N.J., 1999. Functional role of p21 during the cellular response to stress. Gene Expr. 7, 377–385.

Hammond, S.M., Gogliotti, R.G., Rao, V., Beauvais, A., Kothary, R., DiDonato, C.J., 2010. Mouse survival motor neuron alleles that mimic SMN2 splicing and are inducible rescue embryonic lethality early in development but not late. PLoS One 5, e15887. https://doi.org/10.1371/journal.pone.0015887.

Hingorani, R., Bi, B., Dao, T., Bae, Y., Matsuzawa, A., Crispe, I.N., 2000. CD95/Fas signaling in T lymphocytes induces the cell cycle control protein p21cip-1/WAF-1,

which promotes apoptosis. J. Immunol. 164, 4032–4036. https://doi.org/10.4049/jimmunol.164.8.4032.

Hobeika, A.C., Subramaniam, P.S., Johnson, H.M., 1997. IFNalpha induces the expression of the cyclin-dependent kinase inhibitor p21 in human prostate cancer cells. Oncogene 14, 1165–1170. https://doi.org/10.1038/sj.onc.1200939.

Hu, W., Feng, Z., Atwal, G.S., Levine, A.J., 2008. p53: a new player in reproduction. Cell Cycle 7, 848–852. https://doi.org/10.4161/cc.7.7.5658.

Ichijo, H., Nishida, E., Irie, K., ten Dijke, P., Saitoh, M., Moriguchi, T., Takagi, M., Matsumoto, K., Miyazono, K., Gotoh, Y., 1997. Induction of apoptosis by ASK1, a mammalian MAPKKK that activates SAPK/JNK and p38 signaling pathways. Science 275, 90–94. https://doi.org/10.1126/science.275.5296.90.

Jacks, T., Remington, L., Williams, B.O., Schmitt, E.M., Halachmi, S., Bronson, R.T., Weinberg, R.A., 1994. Tumor spectrum analysis in p53-mutant mice. Curr. Biol. 4, 1–7. https://doi.org/10.1016/s0960-9822(00)00002-6.

Jangi, M., Fleet, C., Cullen, P., Gupta, S.V., Mekhoubad, S., Chiao, E., Allaire, N., Bennett, C.F., Rigo, F., Krainer, A.R., Hurt, J.A., Carulli, J.P., Staropoli, J.F., 2017. SMN deficiency in severe models of spinal muscular atrophy causes widespread intron retention and DNA damage. Proc. Natl. Acad. Sci. U. S. A. 114, E2347–E2356. https://doi.org/10.1073/pnas.1613181114.

Janicke, R.U., Sohn, D., Essmann, F., Schulze-Osthoff, K., 2007. The multiple battles fought by anti-apoptotic p21. Cell Cycle 6, 407–413. https://doi.org/10.4161/cc.6.4.3855.

Jiang, P., Du, W., Wang, X., Mancuso, A., Gao, X., Wu, M., Yang, X., 2011. p53 regulates biosynthesis through direct inactivation of glucose-6-phosphate dehydrogenase. Nat. Cell Biol. 13, 310–316. https://doi.org/10.1038/ncb2172.

Kang, K.H., Kim, W.H., Choi, K.H., 1999. p21 promotes ceramide-induced apoptosis and antagonizes the antideath effect of Bcl-2 in human hepatocarcinoma cells. Exp. Cell Res. 253, 403–412. https://doi.org/10.1006/excr.1999.4644.

Kannan, A., Bhatia, K., Branzei, D., Gangwani, L., 2018. Combined deficiency of Senataxin and DNA-PKcs causes DNA damage accumulation and neurodegeneration in spinal muscular atrophy. Nucleic Acids Res. 46, 8326–8346. https://doi.org/10.1093/nar/gky641.

Karimian, A., Ahmadi, Y., Yousefi, B., 2016. Multiple functions of p21 in cell cycle, apoptosis and transcriptional regulation after DNA damage. DNA Repair (Amst) 42, 63–71. https://doi.org/10.1016/j.dnarep.2016.04.008.

Khanna, A.K., Plummer, M., Nilakantan, V., Pieper, G.M., 2005. Recombinant p21 protein inhibits lymphocyte proliferation and transcription factors. J. Immunol. 174, 7610–7617. https://doi.org/10.4049/jimmunol.174.12.7610.

Kitaura, H., Shinshi, M., Uchikoshi, Y., Ono, T., Iguchi-Ariga, S.M., Ariga, H., 2000. Reciprocal regulation via protein-protein interaction between c-Myc and p21(cip1/waf1/sdi1) in DNA replication and transcription. J. Biol. Chem. 275, 10477–10483. https://doi.org/10.1074/jbc.275.14.10477.

Kolb, S.J., Kissel, J.T., 2015. Spinal muscular atrophy. Neurol. Clin. 33, 831–846. https://doi.org/10.1016/j.ncl.2015.07.004.

Kondo, S., Barna, B.P., Kondo, Y., Tanaka, Y., Casey, G., Liu, J., Morimura, T., Kaakaji, R., Peterson, J.W., Werbel, B., Barnett, G.H., 1996. WAF1/CIP1 increases the susceptibility of p53 non-functional malignant glioma cells to cisplatin-induced apoptosis. Oncogene 13, 1279–1285.

Le, T.T., Pham, L.T., Butchbach, M.E., Zhang, H.L., Monani, U.R., Coovert, D.D., Gavrilina, T.O., Xing, L., Bassell, G.J., Burghes, A.H., 2005. SMNDelta7, the major product of the centromeric survival motor neuron (SMN2) gene, extends survival in mice with spinal muscular atrophy and associates with full-length SMN. Hum. Mol. Genet. 14, 845–857. https://doi.org/10.1093/hmg/ddi078.

Lefebvre, S., Burglen, L., Reboullet, S., Clermont, O., Burlet, P., Viollet, L., Benichou, B., Cruaud, C., Millasseau, P., Zeviani, M., et al., 1995. Identification and characterization of a spinal muscular atrophy-determining gene. Cell 80, 155–165. https://doi.org/10.1016/0092-8674(95)90460-3.

Levine, A.J., Oren, M., 2009. The first 30 years of p53: growing ever more complex. Nat. Rev. Cancer 9, 749–758. https://doi.org/10.1038/nrc2723.

Lorson, C.L., Hahnen, E., Androphy, E.J., Wirth, B., 1999. A single nucleotide in the SMN gene regulates splicing and is responsible for spinal muscular atrophy. Proc. Natl. Acad. Sci. U. S. A. 96, 6307–6311. https://doi.org/10.1073/pnas.96.11.6307.

Mallick, S., D'Mello, S.R., 2014. JAZ (Znf346), a SIRT1-interacting protein, protects neurons by stimulating p21 (WAF/CIP1) protein expression. J. Biol. Chem. 289, 35409–35420. https://doi.org/10.1074/jbc.M114.597575.

Matsumura, I., Ishikawa, J., Nakajima, K., Oritani, K., Tomiyama, Y., Miyagawa, J., Kato, T., Miyazaki, H., Matsuzawa, Y., Kanakura, Y., 1997. Thrombopoietin-induced differentiation of a human megakaryoblastic leukemia cell line, CMK, involves transcriptional activation of p21(WAF1/Cip1) by STAT5. Mol. Cell. Biol. 17, 2933–2943. https://doi.org/10.1128/mcb.17.5.2933.

Missero, C., Calautti, E., Eckner, R., Chin, J., Tsai, L.H., Livingston, D.M., Dotto, G.P., 1995. Involvement of the cell-cycle inhibitor Cip1/WAF1 and the E1A-associated p300 protein in terminal differentiation. Proc. Natl. Acad. Sci. U. S. A. 92, 5451–5455. https://doi.org/10.1073/pnas.92.12.5451.

Mullan, P.B., Quinn, J.E., Harkin, D.P., 2006. The role of BRCA1 in transcriptional regulation and cell cycle control. Oncogene 25, 5854–5863. https://doi.org/10.1038/sj.onc.1209872.

Murray, L.M., Beauvais, A., Gibeault, S., Courtney, N.L., Kothary, R., 2015. Transcriptional profiling of differentially vulnerable motor neurons at pre-symptomatic stage in the Smn (2b/−) mouse model of spinal muscular atrophy. Acta Neuropathol Commun 3, 55. https://doi.org/10.1186/s40478-015-0231-1.

Nichterwitz, S., Nijssen, J., Storvall, H., Schweingruber, C., Comley, L.H., Allodi, I., Lee, M.V., Deng, Q., Sandberg, R., Hedlund, E., 2020. LCM-seq reveals unique transcriptional adaptation mechanisms of resistant neurons and identifies protective pathways in spinal muscular atrophy. Genome Res. 30, 1083–1096. https://doi.org/10.1101/gr.265017.120.

Olaso, R., Joshi, V., Fernandez, J., Roblot, N., Courageot, S., Bonnefont, J.P., Melki, J., 2006. Activation of RNA metabolism-related genes in mouse but not human tissues deficient in SMN. Physiol. Genomics 24, 97–104. https://doi.org/10.1152/physiolgenomics.00134.2005.

Pardali, K., Kurisaki, A., Moren, A., ten Dijke, P., Kardassis, D., Moustakas, A., 2000. Role of Smad proteins and transcription factor Sp1 in p21(Waf1/Cip1) regulation by transforming growth factor-beta. J. Biol. Chem. 275, 29244–29256. https://doi.org/10.1074/jbc.M909467199.

Piccolo, M.T., Crispi, S., 2012. The dual role played by p21 may influence the apoptotic or anti-apoptotic fate in cancer. Journal of Cancer Research Updates 1, 189–202. https://doi.org/10.6000/1929-2279.2012.01.02.5.

Porteiro, B., Fondevila, M.F., Delgado, T.C., Iglesias, C., Imbernon, M., Iruzubieta, P., Crespo, J., Zabala-Letona, A., Ferno, J., Gonzalez-Teran, B., Matesanz, N., Hernandez-Cosido, L., Marcos, M., Tovar, S., Vidal, A., Sanchez-Ceinos, J., Malagon, M.M., Pombo, C., Zalvide, J., Carracedo, A., Buque, X., Dieguez, C., Sabio, G., Lopez, M., Aspichueta, P., Martinez-Chantar, M.L., Nogueiras, R., 2017. Hepatic p63 regulates steatosis via IKKbeta/ER stress. Nat. Commun. 8, 15111. https://doi.org/10.1038/ncomms15111.

Porteiro, B., Fondevila, M.F., Buque, X., Gonzalez-Rellan, M.J., Fernandez, U., Mora, A., Beiroa, D., Senra, A., Gallego, R., Ferno, J., Lopez, M., Sabio, G., Dieguez, C., Aspichueta, P., Nogueiras, R., 2018. Pharmacological stimulation of p53 with low-dose doxorubicin ameliorates diet-induced nonalcoholic steatosis and steatohepatitis. Mol Metab 8, 132–143. https://doi.org/10.1016/j.molmet.2017.12.005.

Prokesch, A., Graef, F.A., Madl, T., Kahlhofer, J., Heidenreich, S., Schumann, A., Moyschewitz, E., Pristoynik, P., Blaschitz, A., Knauer, M., Muenzner, M., Bogner-Strauss, J.G., Dohr, G., Schulz, T.J., Schupp, M., 2017. Liver p53 is stabilized upon starvation and required for amino acid catabolism and gluconeogenesis. FASEB J. 31, 732–742. https://doi.org/10.1096/fj.201600845R.

Quinlan, K.A., Reedich, E.J., Arnold, W.D., Puritz, A.C., Cavarsan, C.F., Heckman, C.J., DiDonato, C.J., 2019. Hyperexcitability precedes motoneuron loss in the Smn(2B/−) mouse model of spinal muscular atrophy. J. Neurophysiol. 122, 1297–1311. https://doi.org/10.1152/jn.00652.2018.

Ruggiu, M., McGovern, V.L., Lotti, F., Saieva, L., Li, D.K., Kariya, S., Monani, U.R., Burghes, A.H., Pellizzoni, L., 2012. A role for SMN exon 7 splicing in the selective vulnerability of motor neurons in spinal muscular atrophy. Mol. Cell. Biol. 32, 126–138. https://doi.org/10.1128/MCB.06077-11.

Sareen, D., Ebert, A.D., Heins, B.M., McGivern, J.V., Ornelas, L., Svendsen, C.N., 2012. Inhibition of apoptosis blocks human motor neuron cell death in a stem cell model of spinal muscular atrophy. PLoS One 7, e39113. https://doi.org/10.1371/journal.pone.0039113.

Schellino, R., Boido, M., Borsello, T., Vercelli, A., 2018. Pharmacological c-Jun NH2-terminal kinase (JNK) pathway inhibition reduces severity of spinal muscular atrophy disease in mice. Front. Mol. Neurosci. 11, 308. https://doi.org/10.3389/fnmol.2018.00308.

Schrank, B., Gotz, R., Gunnersen, J.M., Ure, J.M., Toyka, K.V., Smith, A.G., Sendtner, M., 1997. Inactivation of the survival motor neuron gene, a candidate gene for human spinal muscular atrophy, leads to massive cell death in early mouse embryos. Proc. Natl. Acad. Sci. U. S. A. 94, 9920–9925. https://doi.org/10.1073/pnas.94.18.9920.

Seoane, J., Le, H.V., Shen, L., Anderson, S.A., Massague, J., 2004. Integration of Smad and forkhead pathways in the control of neuroepithelial and glioblastoma cell proliferation. Cell 117, 211–223. https://doi.org/10.1016/s0092-8674(04)00298-3.

Sheikh, M.S., Rochefort, H., Garcia, M., 1995. Overexpression of p21WAF1/CIP1 induces growth arrest, giant cell formation and apoptosis in human breast carcinoma cell lines. Oncogene 11, 1899–1905.

Simon, C.M., Dai, Y., Van Alstyne, M., Koutsioumpa, C., Pagiazitis, J.G., Chalif, J.I., Wang, X., Rabinowitz, J.E., Henderson, C.E., Pellizzoni, L., Mentis, G.Z., 2017. Converging mechanisms of p53 activation drive motor neuron degeneration in spinal muscular atrophy. Cell Rep. 21, 3767–3780. https://doi.org/10.1016/j.celrep.2017.12.003.

Simon, C.M., Van Alstyne, M., Lotti, F., Bianchetti, E., Tisdale, S., Watterson, D.M., Mentis, G.Z., Pellizzoni, L., 2019. Stasimon contributes to the loss of sensory synapses and motor neuron death in a mouse model of spinal muscular atrophy. Cell Rep. 29 (3885–3901), e3885 https://doi.org/10.1016/j.celrep.2019.11.058.

Staropoli, J.F., Li, H., Chun, S.J., Allaire, N., Cullen, P., Thai, A., Fleet, C.M., Hua, Y., Bennett, C.F., Krainer, A.R., Kerr, D., McCampbell, A., Rigo, F., Carulli, J.P., 2015. Rescue of gene-expression changes in an induced mouse model of spinal muscular atrophy by an antisense oligonucleotide that promotes inclusion of SMN2 exon 7. Genomics 105, 220–228. https://doi.org/10.1016/j.ygeno.2015.01.007.

Suzuki, A., Tsutomi, Y., Akahane, K., Araki, T., Miura, M., 1998. Resistance to Fas-mediated apoptosis: activation of caspase 3 is regulated by cell cycle regulator p21WAF1 and IAP gene family ILP. Oncogene 17, 931–939. https://doi.org/10.1038/sj.onc.1202021.

Tadesse, H., Deschenes-Furry, J., Boisvenue, S., Cote, J., 2008. KH-type splicing regulatory protein interacts with survival motor neuron protein and is misregulated in spinal muscular atrophy. Hum. Mol. Genet. 17, 506–524. https://doi.org/10.1093/hmg/ddm327.

Tsai, M.S., Chiu, Y.T., Wang, S.H., Hsieh-Li, H.M., Li, H., 2006. Abolishing Trp53-dependent apoptosis does not benefit spinal muscular atrophy model mice. Eur. J. Hum. Genet. 14, 372–375. https://doi.org/10.1038/sj.ejhg.5201556.

Tsao, Y.P., Huang, S.J., Chang, J.L., Hsieh, J.T., Pong, R.C., Chen, S.L., 1999. Adenovirus-mediated p21((WAF1/SDII/CIP1)) gene transfer induces apoptosis of human cervical cancer cell lines. J. Virol. 73, 4983–4990. https://doi.org/10.1128/JVI.73.6.4983-4990.1999.

Wang, X., Zhao, X., Gao, X., Mei, Y., Wu, M., 2013. A new role of p53 in regulating lipid metabolism. J. Mol. Cell Biol. 5, 147–150. https://doi.org/10.1093/jmcb/mjs064.

Wu, C.Y., Whye, D., Glazewski, L., Choe, L., Kerr, D., Lee, K.H., Mason, R.W., Wang, W., 2011. Proteomic assessment of a cell model of spinal muscular atrophy. BMC Neurosci. 12, 25. https://doi.org/10.1186/1471-2202-12-25.

Xu, S.Q., El-Deiry, W.S., 2000. p21(WAF1/CIP1) inhibits initiator caspase cleavage by TRAIL death receptor DR4. Biochem. Biophys. Res. Commun. 269, 179–190. https://doi.org/10.1006/bbrc.2000.2247.

Zeng, Y.X., Somasundaram, K., el-Deiry, W.S., 1997. AP2 inhibits cancer cell growth and activates p21WAF1/CIP1 expression. Nat. Genet. 15, 78–82. https://doi.org/10.1038/ng0197-78.

Zhang, Y., Alexander, P.B., Wang, X.F., 2017. TGF-beta family Signaling in the control of cell proliferation and survival. Cold Spring Harb. Perspect. Biol. 9, a022145 https://doi.org/10.1101/cshperspect.a022145.

Zhang, Z., Lotti, F., Dittmar, K., Younis, I., Wan, L., Kasim, M., Dreyfuss, G., 2008. SMN deficiency causes tissue-specific perturbations in the repertoire of snRNAs and widespread defects in splicing. Cell 133, 585–600. https://doi.org/10.1016/j.cell.2008.03.031.

Zhang, Z., Pinto, A.M., Wan, L., Wang, W., Berg, M.G., Oliva, I., Singh, L.N., Dengler, C., Wei, Z., Dreyfuss, G., 2013. Dysregulation of synaptogenesis genes antecedes motor neuron pathology in spinal muscular atrophy. Proc. Natl. Acad. Sci. U. S. A. 110, 19348–19353. https://doi.org/10.1073/pnas.1319280110.